Design, synthesis and biological evaluation of multitarget hybrid molecules containing NHC-Au(I) complexes and carbazole moieties

A. D'Amato[1, ‡], D. Iacopetta[2, ‡], J. Ceramella[2], R. Troiano[1], A. Mariconda[3, *], A. Catalano[4, *], M. Marra[2], C. Saturnino[3], C. Rosano[5], M.S. Sinicropi[2, ǁ], P. Longo[1, ǁ]

[1] Department of Chemistry and Biology "A. Zambelli", University of Salerno, Via Giovanni Paolo II 132, I-84084 Fisciano (SA), Italy.

[2] Department of Pharmacy, Health and Nutritional Sciences, University of Calabria, Via Pietro Bucci, I-87036 Arcavacata di Rende (CS), Italy.

[3] Department of Science, University of Basilicata, Viale dell'Ateneo Lucano 10, I-85100 Potenza, Italy.

[4] Department of Pharmacy-Drug Sciences, University of Bari "Aldo Moro", Via Orabona 4, 70126 Bari, Italy.

[5] U.O. Proteomica e Spettrometria di Massa, IRCCS Ospedale Policlinico San Martino, Largo R. Benzi 10, 16132, Genova, Italy.

[‡] considered co-first authors.

[*]correspondence to: annaluisa.mariconda@unibas.it; s.sinicropi@unical.it

[ǁ]considered co-senior authors.

Abstract

N-heterocyclic carbenes (NHCs) represent suitable ligands for rapid and efficient drug design, because they offer the advantage of being easily chemically modified and can bind several substituents, including transition metals as, for instance, gold derivatives. Gold-NHC complexes possess various biological activities and were demonstrated good candidates as anticancer drugs. Besides, carbazole derivatives are characterized by various pharmacological properties, such as anticancer, antibacterial, anti-inflammatory, and anti-psychotropic. Amongst the latter, N-thioalkyl carbazoles were proved to inhibit cancer cells damaging the nuclear DNA, through the inhibition of human topoisomerases. Herein, we report the design, synthesis and biological evaluation of nine new hybrid molecules in which NHC-Au(I) complexes and *N*-alkylthiolated carbazoles are linked together, in order to obtain novel biological multitarget agents. We demonstrated that the lead hybrid complexes possess anticancer, anti-inflammatory and antioxidant properties, with a high potential as useful tools for treating distinct aspects of several diseases, amongst them cancer.

Keywords: *N*-heterocyclic carbenes; *N*-alkylthiolated carbazoles; hybrid molecules; anticancer; antioxidant; anti-inflammatory.

1.Introduction

In recent years, there was an increased interest toward the multitarget and poly-pharmacologic approach for many diseases, including cancer, in order to obtain new, more effective and selective drugs with fewer side effects and able to face the resistance phenomena onset [1]. The clinical practice of combining two or more drugs together produced some good therapeutic results, but the patient compliance is a fundamental requirement. Besides, the use of co-formulations and, most importantly, the development of hybrid or chimeric molecules, able to target different pathways involved in the onset and development of cancer, are becoming very attractive approaches in medicinal chemistry [2]. Particularly, the advancement of effective conjugate chemistry methods represents a fruitful way towards the improvement of drugs quality, in terms of potency and of variety of targets, since it is advantageous to link together the already known pharmacophores obtaining new chimeric entities with new or ameliorated features [3]. Thus, the aim of the present work was to design and synthetize nine new hybrid molecules, containing gold-*N*-heterocyclic carbenes (NHC-Au(I)) complexes and *N*-alkylthiolated carbazoles linked together, in order to obtain novel agents with multiple biological activities. This idea raises from our long-lasting experience in the synthesis and biological evaluation of NHC-Au(I) complexes and carbazole derivatives [4-11]. The former have attracted the interest of many researchers because of their chemical versatility and a plethora of applications in various fields, the latter were derived from the naturally occurring alkaloid ellipticine and, during the years, myriad of derivatives were chemically obtained and reported for their multiple properties, including anticancer, antibacterial, anti-inflammatory, and anti-psychotropic [12]. To name but few, gold-NHC complexes were proved to be more effective with respect to *Cis*platin, with a higher selectivity toward several cancer cell lines [13], and represent a valid and promising alternative for overcoming the resistance phenomena onset. Moreover, they were found to be particularly effective as environmentally sustainable catalysts, producing different intermediates necessary for the chemical and pharmaceutical industry [14]. Besides, the carbazole scaffold is one of the main studied nitrogen-containing heterocyclic pharmacophores in medicinal chemistry, because of its fascinating drug-like properties and extraordinary biological activities [12, 15]. Although several carbazole containing-drugs were approved for the treatment of various diseases, included cancer, their therapeutic potential was not yet fully explored and exploited; Indeed, a renewed interest in discovering and developing new carbazole analogues, more effective and with a minor toxicity, was recorded [16]. In the present study, the biological evaluation of the new hybrid complexes produced different exciting outcomes, since the most active leads were found able to selectively decrease the viability of two different models of breast cancer cells, namely MCF-7 and MDA-MB-231 cells, provoking DNA damage through the inhibition of the human topoisomerase I (hTopoI). Contemporaneously, they were also

good anti-inflammatory and antioxidant agents, inhibiting the NO production in LPS-stimulated RAW 264.7 macrophages and scavenging the ROS production, experimentally induced in BALB/3T3 murine fibroblasts. *In silico* simulations toward the hTopoI and inducible nitric oxide synthase (iNOS) were performed, in order to gain further insights about the underlying mechanism. Furthermore, the individuated leads were also able to modulate the iNOS and TNFα intracellular expression, *via* the modulation of NF-kB transcriptional activity. Overall, combining two important entities produced new hybrid complexes, paving the way for further design and synthesis of drugs gifted of multiple pharmacological properties, and with high potential for treating cancer and its multiple aspects as, for instance, exacerbated inflammatory and oxidative stress conditions.

2.Results and discussion

2.1.Chemistry

Chloride gold(I) complexes stabilized by *N*-heterocycle carbene ligands having a carbazole derivative as a substituent of one of the nitrogen atoms, as well as gold(I) complexes with NHC ligands and a carbazole derivative as counterion have been synthesized and characterized. These hybrid complexes have been tested as antitumoral, anti-inflammatory and antioxidant agents, obtaining very interesting results. Complexes **AuL1-AuL4** display Au(I) stabilized by an N-heterocyclic carbenic ligand bearing an alkyl-carbazole substituent on one nitrogen atom and 2-phenyl-2-hydroxy-ethyl group on the other nitrogen. The counter-ion of the metal center is a chloride. On the other hand, complexes **AuL7-AuL10** exhibit the Au(I) supported by a neutral ligand, *i.e.*: N-heterocyclic carbenic ligand featuring a methyl group on one nitrogen atom and (2-hydroxy-2-phenyl)ethyl group on the other, and an S-alkyl-carbazole acting as the anionic ligand (Figure 1). These two classes of compounds could highlight whether to have a more effective biological activity it is preferable for the carbazole to be stably linked (covalent bond) to the *N*-heterocyclic ancillary ligand or rather for it to be a more labile ligand such as the one represented by the bond between the thiolate bearing the *N*-alkyl-carbazole group and the metal center The complex **AuCS3** was synthesized as a negative control to prove that the *N*-heterocyclic carbenic ligand is essential to have good biological activity (Scheme 1).

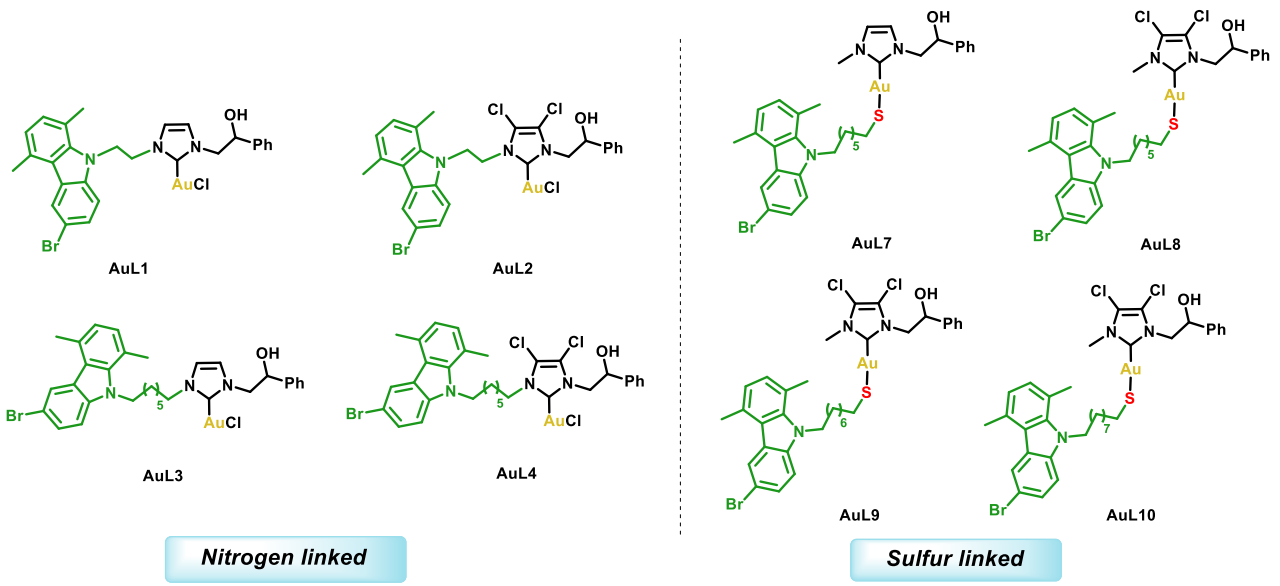

Figure 1. New gold NHC complexes synthesized and studied in this work.

Complexes **AuL1-AuL4** were synthesized as reported in Scheme 1. At first, we tried to synthesize bromoalkyl-*N*-carbazoles **C2-C5** starting from 5-bromoindole, which was reacted with 2,5-hexanedione in the presence of *p*-toluensulfonic acid to give 6-bromo-1,4-dimethyl-9*H*-carbazole (**C1**). This starting material reacts with the appropriate linear α,ω-dibromoalkane producing (*N*-ethyl-2-bromide)-6-bromo-1,4-dimethyl-carbazole (**C2**), (*N*-heptyl-7-bromide)-6-bromo-1,4-dimethyl-carbazole (**C3**), (N-octyl-8-bromide)-6-bromo-1,4-dimethyl-carbazole (**C4**) and (*N*-nonyl-9-bromide)-6-bromo-1,4-dimethyl-carbazole (**C5**). On the other hand, *N*-heterocyclic carbene proligands (**L1 and L2**) were obtained for reaction of (*N*-(2-phenyl-2-hydroxyethyl))-imidazole (**P1**) or (*N*-(2-phenyl-2-hydroxyethyl))-4,5-dichloro-imidazole (**P2**), produced by reaction of imidazole or 4,5-dichloroimidazole with styreneoxide, with (**C2**) respectively.

(**L3**) and (**L4**) were obtained by reaction of (**C3**) with (*N*-(2-phenyl-2-hydroxyethyl))-imidazole (**P1**) or (*N*-(2-phenyl-2-hydroxyethyl))-4,5-dichloro-imidazole (**P2**), respectively (see Scheme 1).

Complexes **(AuL1-4)** were obtained by reaction of chloro(dimethylsulfide)gold(I) with proligands **(L1-4)**, respectively.

Complex (**AuL7**) derives from [*N*-(2-hydroxy-2-phenylethyl)-*N*′-(methyl)-imidazole-2-ylidene]gold(I)chloride (**AuL5**) by replacement of the chloride ion with 1-bromo- 4,6-dimethyl-9-heptyl-thiolate anion **(CS3)** in the presence of triethylamine. While the complexes (**AuL8**), (**AuL9**) and (**AuL10**) are derived from [4,5-dichloro-*N*-(2-hydroxy-2-phenylethyl)-*N*′-(methyl)-imidazole-2-ylidene]gold (I)chloride (**AuL6**) by replacement of the halide anion with the appropriate 1-bromo-4,6-dimethyl-9-alkyl-thiolate anion (**CS3-CS5**). The synthesis and biological activity of **AuL5** and

AuL6 has already been reported in the literature [5, 17, 18]. The thiol derivatives **CS3**, **CS4**, and **CS5** were obtained by reaction with thiourea of **C3, C4**, and **C5**, respectively, as reported in the experimental part. Complex (**AuCS3**) was synthesized by direct reaction of $(CH_3)_2SAuCl$ with (**CS3**).

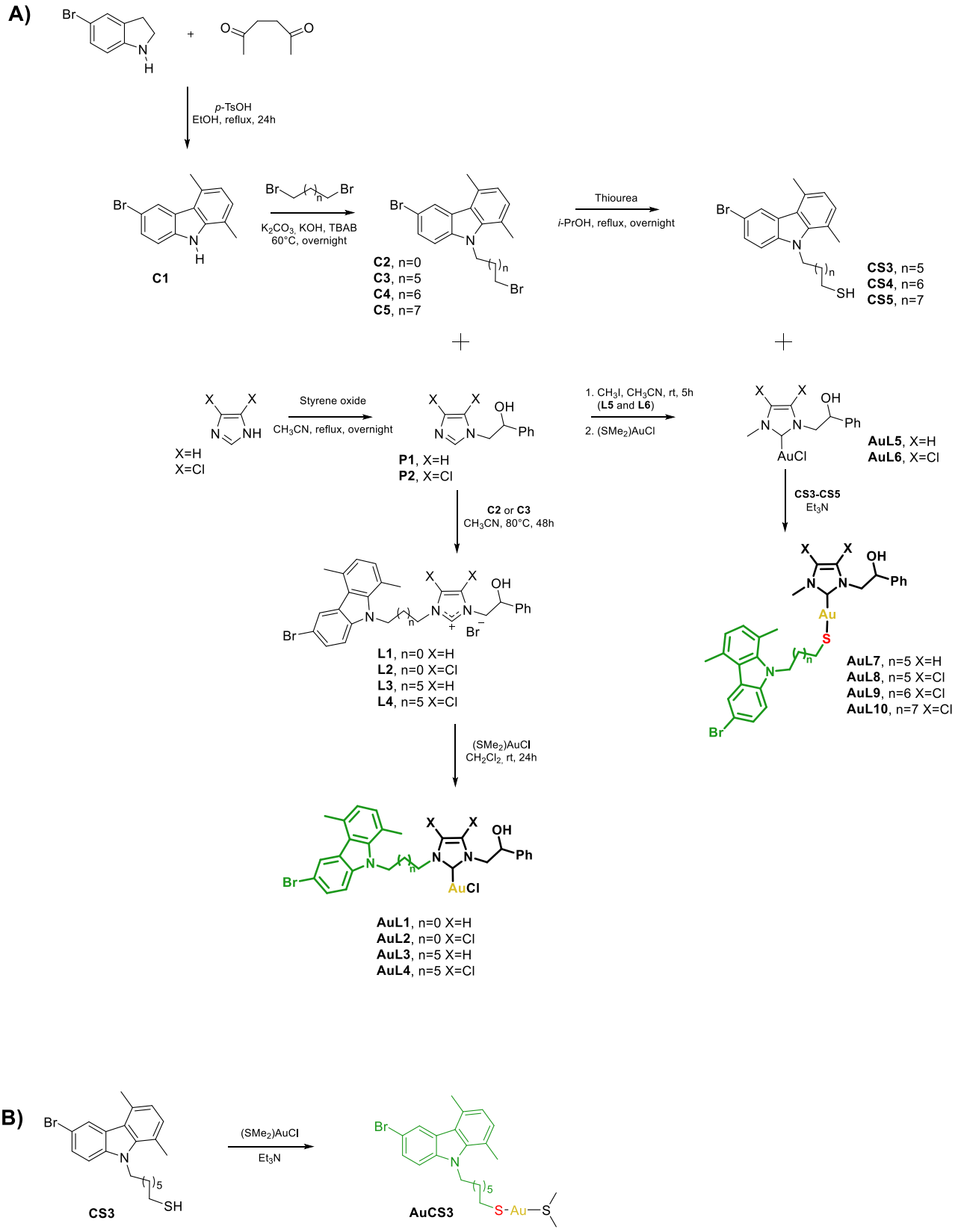

Scheme 1. A) Synthesis of complexes (**AuL1-4** and **AuL7-10**). **B)** Synthesis of negative control **AuCS3**.

The carbazole **C1** and the carbazole derivatives **C2-C5** and **CS3-CS5** were characterized by ^{1}H and ^{13}C-NMR and mass spectrometry. The spectra obtained are perfectly consistent with what was expected and with what has already been reported in the literature [6].

The **L1-L4** pro-ligands were characterized by NMR analysis and MALDI mass spectrometry (see experimental section). The proton on the carbocationic carbon is very characteristic and resonates at 9.00 ppm for **L1**, at 8.28 ppm for **L2**, at 9.66 for **L3**, and at 10.68 for **L4**. In the ^{13}C NMR spectra the carbocationic carbon is the one that resonates at the lowest field, *i.e.:* between 141.19 and 139.18 ppm. The mass spectra of all these proligands give the signal corresponding to the cationic portion (see section 4 and Supporting Information).

NMR spectra of the metal complexes were recorded in $CDCl_3$ at room temperature. The ^{1}H and ^{13}C NMR spectra show the predictable signals. In ^{1}H NMR of the complexes **AuL1** and **AuL2** the signals of the protons of methylene of the imidazole's alkyl-chain bonded to the nitrogen of imidazole ring resonate as a triplet at 3.56 ppm, whereas the same protons in the complexes **AuL3** and **AuL4** the triplet resonate at 4.48 ppm. In the ^{13}C NMR spectra, the signals of carbene carbons are at 199.76 ppm for **AuL1** and at 204.44 for **AuL2**, whereas those for **AuL3** and **AuL4** resonate at 173.49 and 175.05 ppm, respectively.

^{13}C NMR spectra of **AuL7** shows the carbene signal at 170.88 ppm, whereas the carbene signals of **AuL8, AuL9** and **AuL10** are at 171.86, 171.49 and 172.03 ppm, respectively.

It should be noted that, as widely reported in the literature for similar compounds based on diffractometric and mass spectrometric analyses [19-21], in solution the N-heterocyclic gold complexes of carbene give rise to the following equilibrium:

$$[(NHC)_2Au]^+[AuX_2]^- \rightleftharpoons 2(NHC)AuX$$

Obviously the ^{13}C NMR analysis of the two species can give different signals for the carbenic carbons, thus, the equilibrium is more shifted towards the formation of ionic species in **AuL1** and **AuL2** and correspondingly the signals of the carbenic carbons resonate at very low fields (around 200 ppm) [22, 23]. The equilibrium is more shifted to the right, i.e. towards the neutral species for the **AuL3, AuL4, AuL7, AuL8, AuL9** and **AuL10** complexes and their carbenic carbons resonate at higher fields (around 170 ppm) [18, 23-25]. The MALDI-MS analyses confirm what is highlighted by the ^{13}C NMR data, in fact **AuL1** and **AuL2** give signals attributable to complexes in which the gold is linked to two carbene ligands, while the mass spectra of the complexes **AuL3, AuL4, AuL7, AuL8, AuL9**

and **AuL10** highlight a structure in which the metal is bonded to a single N-heterocyclic carbenic ligand.

2.2. Anticancer activity

The new synthesized complexes were tested for their potential anticancer activity against three different breast cell lines, namely the ER-positive MCF-7 and the triple negative MDA MB-231 breast cancer cells and the normal human mammary epithelial cell line MCF-10A. MTT assay was employed for these studies, and the results were expressed as IC_{50} values, resumed in Table 1. The best anticancer activity was obtained for complexes **AuL8**, **AuL9** and **AuL10** toward both the breast cancer cells, but with IC_{50} values of about the half against the MCF-7 cells (3.6±0.5, 3.5±0.2 and 2.7±0.3 μM, respectively) with respect to those obtained for MDA-MB-231 cells (6.4±0.4, 6.3±0.7 and 6.1±0.2 μM, respectively). The values are very close each other and these results were easily foreseeable, since the above-mentioned complexes differ only in the length of the thioalkyl chain bridging the carbazole core with the NHC-gold scaffold of 7, 8 and 9 methylene groups for **AuL8**, **AuL9** and **AuL10** respectively. Thus, it can be deduced that, for these complexes, the length of the thioalkyl chain is quite irrelevant for the anticancer activity. The complexes **AuL8**, **AuL9** and **AuL10** were also found the most selective towards the breast cell lines used, since their respective indices were of 6.4, 6.3 and 11.2 for the MDA-MB-231 cells, and 3.6, 3.6 and 7.9 for the MCF-7 cells, respectively, as visible in Table 2, being the complex **AuL10** the most selective overall. Interestingly and quite unexpected, complex **AuL7** did not exhibit any anticancer activity, with IC_{50} values >50 μM against all the adopted cells. The latter complex does not have the two chlorine substituents at the NHC core, which were, instead, present in the complex **AuL8** that was one of the most active. Additionally, complex **AuCS3**, in which the thioalkyl chain is the same of complex **AuL8** but gold is linked to dimethyl sulphur substituent (NHC core is lacking), did not possess any activity. Then, these results indicated that the presence of the NHC core is required for the anticancer activity and that the two chlorines are also determinant. Going ahead, the NHC core is very relevant for the anticancer activity, as well as for the position of the carbazole portion. As can be seen in Figure 1 and Table 1, complexes **AuL3** and **AuL4**, despite having a methylene chain of seven atoms (similarly to complex **AuL8)** and two chlorines as substituents of NHC nucleus (complex **AuL4**), possess the carbazole scaffold as substituent of a nitrogen atom of the NHC core and resulted inactive. Indeed, the complex **AuL3** IC_{50} values are of 48.3±2.6 and 49.1±1.6 μM and the complex **AuL4** IC_{50} values are both higher than 50 μM, for MCF-7 and MDA-MB-231 respectively. Finally, complexes **AuL1** (IC_{50} values of 31.4±0.5 and 40.7±0.9 μM, for MCF-7 and MDA-MB-231 cells, respectively) and

AuL2 (IC_{50} values of 34.1±1.3 and >50 μM, for MCF-7 and MDA-MB-231 cells, respectively) exhibited a low anticancer activity overall, but are better than their respective structural analogues, complexes **AuL3** and **AuL4**, respectively. It should be highlighted that these analogues (**AuL1** and **AuL2**) present a short alkylic chain, which could contribute to slightly improve the anticancer activity whether compared to the analogues having longer chains, even though not at the same level of the most active complexes. As reference molecules, we adopted both Ellipticine and *Cis*platin. Their respective IC_{50} values are reported in Table 1, where it can be deducted that the most active complexes (**AuL8-10**) showed a better cytotoxic profile than them.

Table 1. IC_{50} values, expressed in μM, for the studied complexes (**AuL1-10** and **AUCS3**) and the reference drugs, on three breast cell lines, cancerous and normal, (MCF-7, MDA-MB-231, MCF-10A). The values are the mean ± standard deviation of three different experiments, performed trice.

	IC_{50} (μM)		
	MCF-7	**MDA-MB-231**	**MCF-10A**
AuL1	31.4±0.5	40.7±0.9	>50
AuL2	34.1±1.3	>50	>50
AuL3	48.3±2.6	49.1±1.6	>50
AuL4	>50	>50	>50
AuL7	>50	>50	>50
AuL8	3.6±0.5	6.4±0.4	23.1±1.2
AuL9	3.5±0.2	6.3±0.7	22.1±1.1
AuL10	2.7±0.3	6.1±0.2	30.2±1.4
AuCS3	>50	>50	>50
***Cis*platin**	34.3±1.0	27.3±1.1	>50
Ellipticine 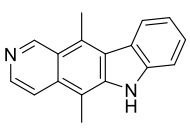	1.3±0.4	1.8±1.0	1.2±0.6

Table 2. Selectivity Index (SI) of the tested complexes, *Cis*platin and Ellipticine

	SI	
	MDA-MB-231	**MCF-7**
AuL1	>1.6	>1.2
AuL2	>1.5	>1.0
AuL3	>1.0	>1.0
AuL4	>1.0	>1.0
AuL7	>1.0	>1.0
AuL8	**6.4**	**3.6**
AuL9	**6.3**	**3.5**
AuL10	**11.2**	**4.9**
AuCS3	>1.0	>1.0
***Cis*platin**	>1.5	>1.8
Ellipticine	0.9	0.7

2.3.DNA damage and inhibition of human topoisomerase I

It is well known that both the NHC-gold complexes and carbazole derivatives may exert their anticancer ability by activating several intracellular signals leading to cancer cells death. In particular, they can induce DNA damage through the interference with pivotal proteins [6, 7, 26]. Thus, aiming at evaluating whether the individuated lead complexes, **AuL9** and **AuL10** induce MCF-7 cells death damaging genomic DNA, a TUNEL assay was performed. Briefly, cells were treated with complexes **AuL9** or **AuL10** for 24 h, at a concentration equal to their respective IC_{50} values, then processed as described in section 4. Figure 2 depicts the obtained outcomes, where is possible to see that MCF-7 cells treated with **AuL9** or **AuL10** have their DNA hardly damaged, as indicated by the evident green nuclear fluorescence (Figure 2, panels B, **AuL9** or **AuL10**) that perfectly superposes with the blue one (Figure 2, panels A, DAPI staining of cells nuclei, and panels C, overlay). Contrarily, MCF-7

cells exposed to DMSO (vehicle, CTRL) did not show DNA damage, since no green nuclear fluorescence was visible (Figure 2, panels B, CTRL).

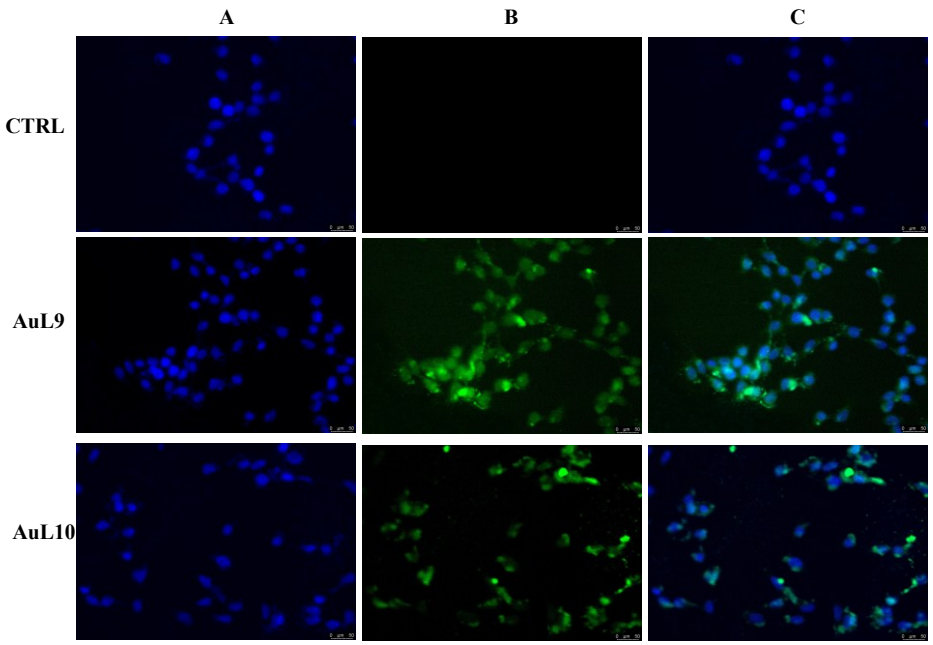

Figure 2. TUNEL assay. MCF-7 breast cancer cells were treated for 24 h with **AuL9** or **AuL10**, at their IC_{50} values, or vehicle (CTRL). Cells were then subjected to rTdT enzyme reaction, in presence of labeled nucleotides, then images were acquired at 20x magnification using an inverted fluorescence microscope. Panels A: DAPI ($\lambda_{ex}/\lambda_{em}$ = 350/460 nm); panels B: CF^{TM}488A ($\lambda_{ex}/\lambda_{em}$ = 490/515 nm) Panels C: merge channels. Representative fields are shown (experiments number = 3).

DNA damage induction is one of most pursued strategy in precision cancer therapy, and a more detailed understanding of the mechanisms underlying the cancer impairment pathways is useful for a selective inhibition of its growth and progression [27]. Different intracellular pathways may trigger DNA damage [28], however our long-lasting experience in studying compounds, able to selectively block important enzymes involved in cancer onset and progression, led us to investigate whether the leads may interfere with one of this key-players, *viz*. the human topoisomerase I (hTopoI). The latter is responsible for the DNA topology integrity control in different stages of its metabolism and is strongly implied in sustaining cancer growth [29]. Thus, a hTopoI relaxation inhibition assay was performed for testing the ability of our leads to block this enzyme, considering that this event induces DNA damage and, consequently, cell death [30]. In short, hTopo I was exposed to **AuL9** or **AuL10** for 1 hour at 1 μM, using the supercoiled DNA (SC DNA) as a substrate, and *Cis*platin and Ellipticine as reference molecules, since our complexes possessed both the moieties in their structures. After

have been further processed (see section 4 for details), the reaction products were loaded on to the agarose gel and electrophoresed. Figure 3 shows the obtained results, interpreted as it follows: i) both the leads **AuL9** and **AuL10** totally blocked the hTopo I activity (already at 1 μM), as evidenced by the uncut plasmid band at the bottom of the gel (lanes 4 and 5); ii) hTopo I full activity was obtained under DMSO exposure (vehicle, less than 0.1 %), as negative control, where the relaxed plasmid topoisomers are present (lane 3); iii) *Cis*platin and Ellipticine inhibited the hTopoI activity, as well, with some distinctions, since *Cis*platin was active only at 50 μM (lane 7) and at 1 μM the relaxation activity was retained (lane 6), whereas Ellipticine was active even at 1 μM, but with the known intercalative capacity (lane 8). Relaxed and SC DNA plasmid were used as markers (Figure 3, lanes 1 and 2, respectively).

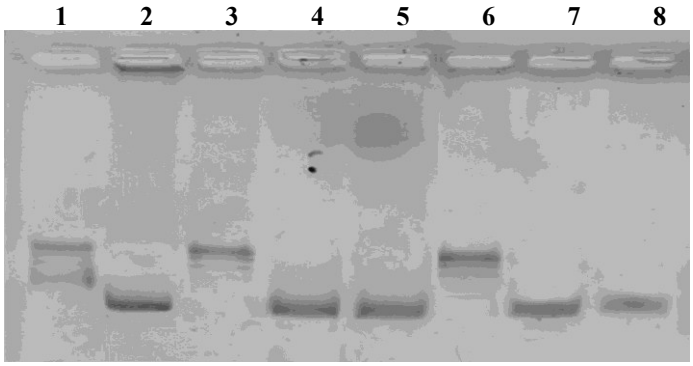

Figure 3. Human topoisomerase I relaxation inhibition assay. Supercoiled DNA was incubated with or without human topoisomerase I, in the absence or presence of **AuL9**, **AuL10**, *Cis*platin, Ellipticine. 1: relaxed marker; 2: super coiled pHOT DNA; 3: DMSO (vehicle as negative control); 4 and 5: **AuL9** and **AuL10**, 1 μM, respectively; 6 and 7: *Cis*platin, 1 and 50 μM, respectively; 8: Ellipticine, 1 μM.

Finally, *in silico* simulations (Figure 4) were also performed in order to gain more information about the inhibitory activity of our leads against the hTopoI. Our molecules are placed in two different areas, both belonging to the region where DNA binds. Complex **AuL9** forms hydrogen bond with Asn352, hydrophobic interactions with residues Phe 361 and Met 428, a halogen bond between the bromide moiety and residue Arg 375 and a π–π stacking with residue Trp 416. Finally, complex **AuL10** adopts a very similar binding mode to the one of complex **AuL9** sharing the same halogen bond and π–π stacking, and forming a hydrogen bond with residue Asn 419 and hydrophobic interactions with Phe 361 and the hydrophobic atoms of Lys 425 side chain. The docking energies are reported in table 3.

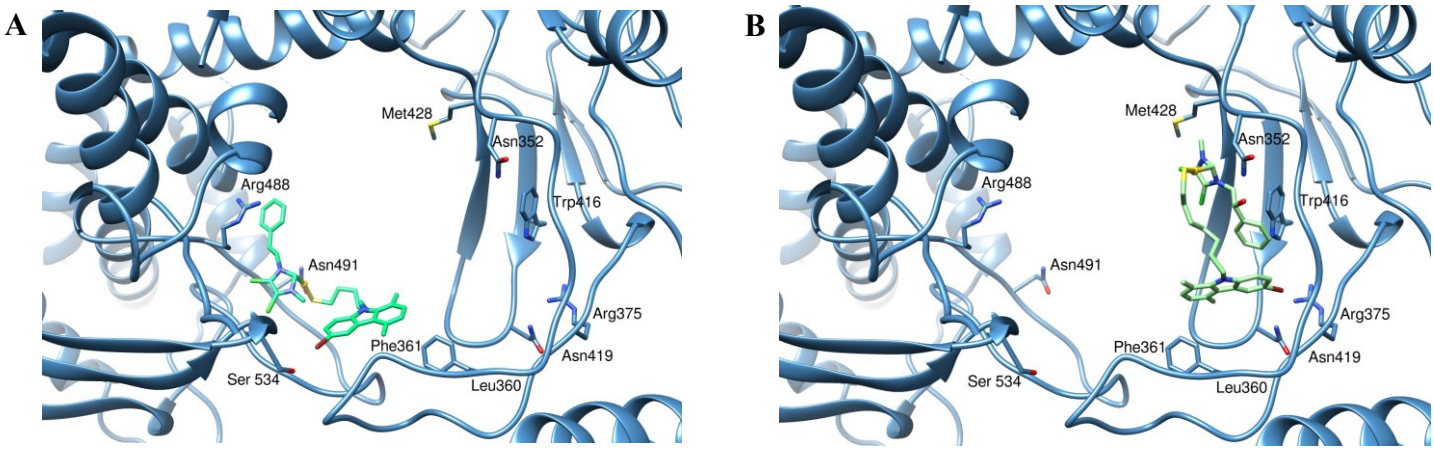

Figure 4: Binding modes to hTopoI (cyan ribbons) of the tested ligands (colored sticks). In panels **A** and **B,** the complexes formed by hTopoI and ligands **AuL9** and **AuL10**, respectively, are shown.

Table 3. Binding energies and affinities of the tested complexes to hTopoI

Compound	Binding Energy (Kcal/mol)	Ki (μM)
AuL9	-7.59	2.72
AuL10	-6.96	7.95

2.4.Anti-inflammatory activity

The new synthesized hybrid complexes were tested for their anti-inflammatory activity by the means of a Griess-based assay. Briefly, the ability of inhibiting the nitric oxide (NO) production in lipopolysaccharide (LPS)-stimulated murine macrophages RAW 264.7 was measured after 24h of treatment (see section 4, for further details). As positive control, we adopted the nonsteroidal anti-inflammatory drug (NSAID) indomethacin (Ind) at the same concentrations used for the tested complexes, namely 5 and 10 μM, and results are resumed in Figure 5. As it is possible to infer, Ind and some of the tested complexes produced a dose-dependent inhibition of NO production in LPS-stimulated RAW 264.7 cells. Particularly, under Ind treatment, an inhibition of NO synthesis of about 8 and 23%, at 5 and 10 μM respectively, was obtained. With the exception of complex **AuL7**, which does not produce any effect at both the concentrations, complexes **AuL1-4**, **AuL8** and **AuCS3** were able to slightly reduce the NO production at 10 μM (ranging from 2 to 9%) concentration, even though

with values lower than, or comparable to, those observed with Ind at 5 μM. Instead, the complexes **AuL9** and **AuL10** exhibited a significant higher inhibitory activity toward the NO synthesis, with respect to Ind at both the dosages. Particularly, the complex **AuL10** was found the most active, inhibiting the NO production of about the 33 and 57% at 5 and 10 μM, respectively, and the complex **AuL9** produced about the 19 and 38% of NO inhibition, at 5 and 10 μM, respectively. It can be easily concluded that both the most active complexes possessed a better anti-inflammatory activity, as NO inhibition, in LPS-stimulated RAW 264.7 macrophages than Ind. In order to be sure that the effect is ascribable to the NO production reduction in viable macrophages, MTT assays were preliminary conducted, under the same experimental conditions adopted for the Griess assay. As noticeable from Figure 6, none of the complexes, nor the reference compound (Ind), affected cells viability, in a significant manner, with respect to the LPS-treated cells, used for comparison.

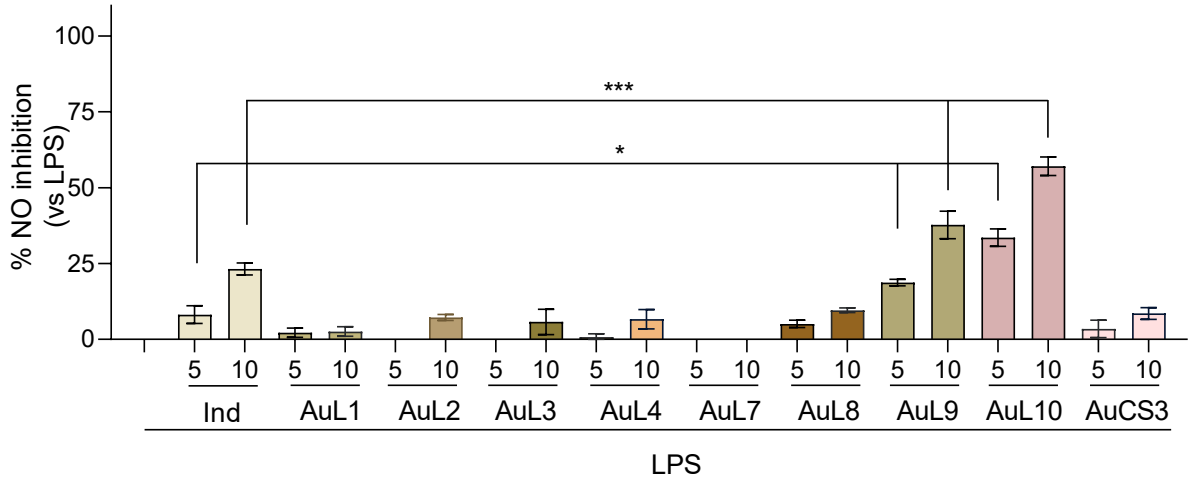

Figure 5. Anti-inflammatory activity in terms of NO production inhibition (%), measured *in vitro*, using the murine macrophages RAW 264.7. NO production was induced by LPS (1 μg/mL). Indomethacin (Ind) and all the complexes were used at the concentrations of 5 and 10 μM, for 24h. Ind *vs* **AuL9** or **AuL10**, *p<0.1, ***p<0.001.

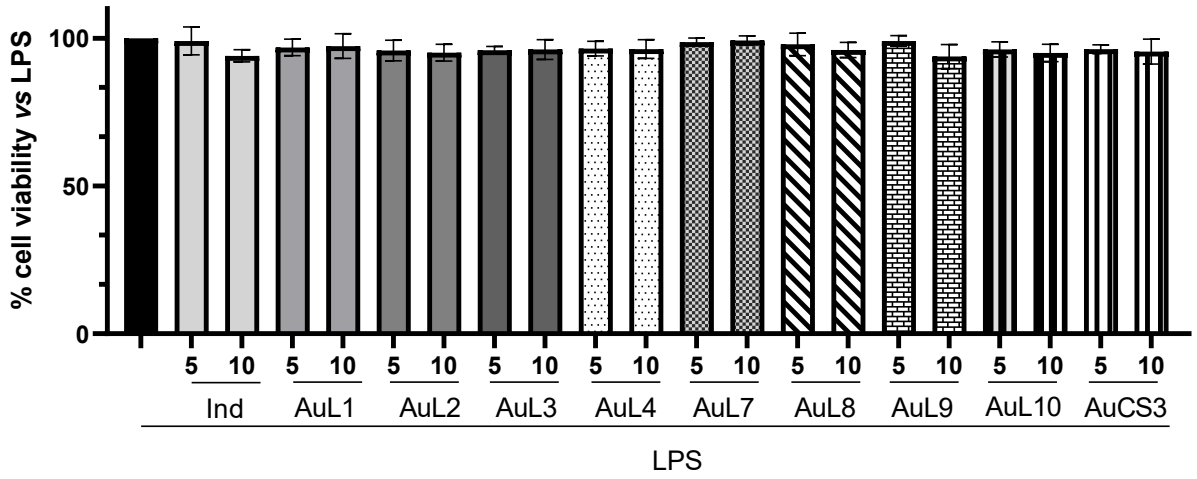

Figure 6. MTT assays were performed (at 5 and 10 μM, for 24 h), in order to verify the effect on RAW 264.7 cells viability of Ind and the tested complexes. Data were plotted as % of cell viability with respect to LPS-only treatment (1 μg/mL). Columns ± SD are reported.

Additionally, thanks to molecular docking simulations we evaluated the most probable binding modes of the most active complexes described above (Figure 7) and iNOS. The analysis of the docking simulations indicated that, among the analyzed complexes, **AuL8** and **AuL10** were more likely able to dock to iNOS forming hydrogen bonds and hydrophobic interactions. For all our complexes, a possible binding site lies in proximity of the protein heme (Figure 6, panel A), almost superposed to the crystallographic binding site of the molecule O-(5-methyl-2-nitrophenyl)-D-tyrosinamide (YWO) [31]. The complex **AuL8** binds the protein forming hydrogen bonds with the heme carboxylic group and protein residues Asn 348 and Glu 371, and hydrophobic interactions with the heme plane and the side chains of residues Ser 256, Pro 344 and Tyr 485. Finally, the gold atom stands mid-way between the oxygen atom of a carboxylic group of the heme and the oxygen atom of the residue Gln 257 side chain (Figure 7, panel B). In the same pose, **AuL9** forms the same hydrogen bonds and hydrophobic interactions than **AuL8** (Figure 7, panel C). **AuL10** (Figure 7, panel D) lays more deeply in the heme binding pocket with respect with the previous two complexes, forming hydrogen bonds with the heme carboxylic group and with the protein residues Ser 256, Gln 257, Glu 371, Asn 266 and Thr 583. The ligand is further stabilized by a halogen bond between its bromide moiety and the carboxylate of Gln 486 and hydrophobic interactions with residues Ala 276, Phe 280 and Pro 344. In this case, the gold atom is bound to the heme carboxylate, but not with Gln 257. Panels E and F show the binding modes of Ind and of YWO respectively.

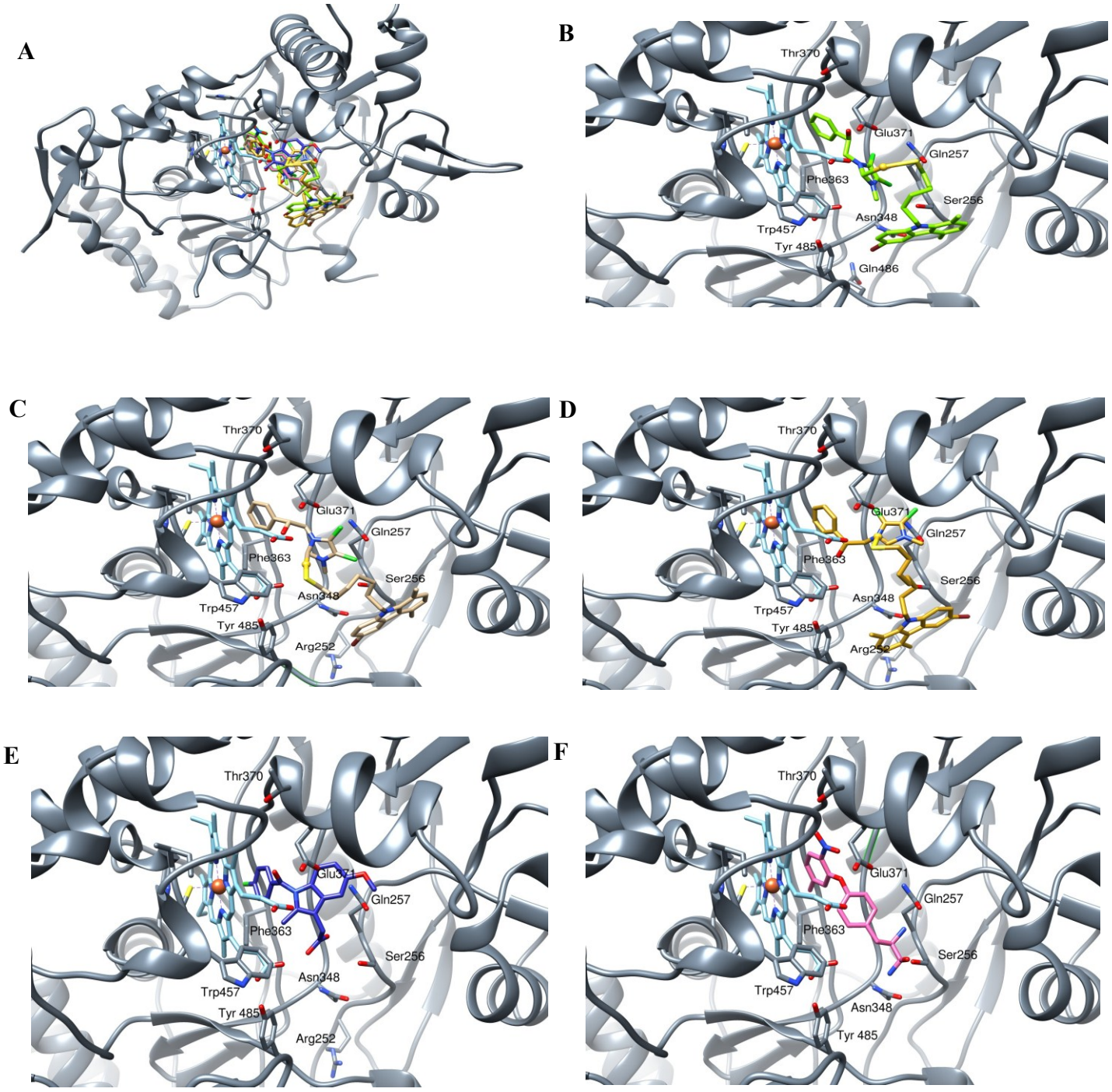

Figure 7. Different binding modes to iNOS (gray ribbons) of the tested ligands (colored sticks) are superposed and showed in panel **A**. In details, Panel **B** reports the position adopted by complex **AuL8** (green sticks) in front of the heme moiety (cyan sticks), Panels **C**, **D** and **E**, show the results of the docking simulations of **AuL9**, **AuL10** and Ind (tan, gold and blue sticks) to iNOS respectively. Panel

F depicts the structure of iNOS complexed with the ligand YWO (pink sticks), as determined by X-ray crystallography (PDB code 4UX6).

Binding energies for the three compounds are reported in Table 4.

Table 4. Binding energies and affinities of the tested compounds to iNOS.

Compound	Binding Energy (Kcal/mol)	Ki (μM)
AuL8	-7.71	2.25
AuL9	-7.95	1.49
AuL10	-9.26	0.163
Ind	-9.53	0.103

Once established the inhibitory ability toward the NO synthesis in RAW 264.7 macrophages, the inducible nitric oxide synthase (iNOS) expression under LPS stimulation and **AuL9** or **AuL10** treatment was investigated, as well, performing immunostaining assays. Thus, RAW 264.7 cells were treated for 24 hours with DMSO (vehicle, negative control), or LPS or co-treated with LPS (1 μg/mL) and Ind (positive control) or the lead complexes (**AuL9** or **AuL10)**. All the compounds were used at the concentration of 5 μM. The obtained outcomes are visible in Figure 8A, where it is noticeable the induced expression of iNOS in LPS-stimulated macrophages, which is higher with respect to the vehicle-treated cells, as expected (panels B, red fluorescence). Furthermore, the co-treatment with Ind was able to reduce the iNOS protein expression, as already reported [32, 33]. Most importantly, a net and higher reduction was recorded under the lead complexes exposure, indeed **AuL9** and **AuL10** were able to reduce iNOS expression with higher efficacy than Ind, under the same experimental conditions (panels B). Taken together, these results suggest that both the lead complexes possess a better inhibitory activity against the iNOS with respect to Ind, decreasing, at the same time, the iNOS expression induced by the LPS treatment. Fluorescence quantification was also reported (Figure 8B).

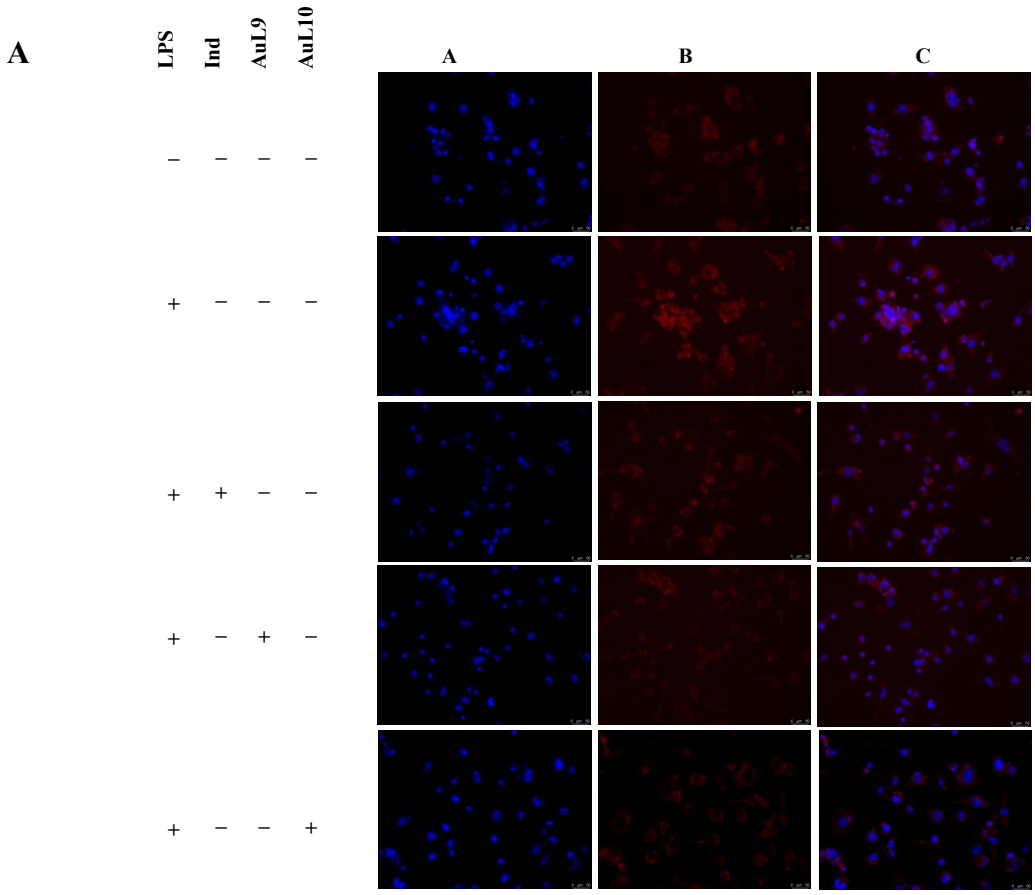

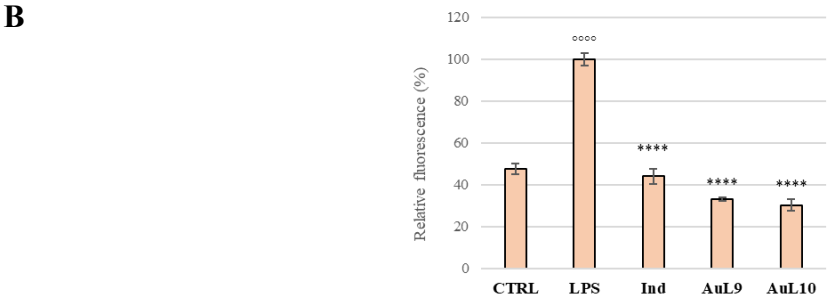

Figure 8. A) semi-quantitative detection of iNOS expression through immunofluorescence assays. RAW 264.7 cells were exposed to DMSO (vehicle), or LPS (1 µg/mL), or co-treated with LPS and Ind or **AuL9** or **AuL10** Panels A, DAPI (λex/em =350/460 nm); panels B, AlexaFluor®568 (λex/em = 644/665 nm); panels C, overlays. Images are representative of three independent experiments and were acquired at 20x. B) ImageJ software was used for fluorescence quantification and results were then graphed; Ind, **AuL9** and **AuL10** vs LPS, ****p<0.0001, LPS vs CTRL, °°°°p<0.0001.

2.5.Inhibition of NF-kB activation in MDA-MB-231 and RAW 264.7 cells

It is reported that the inhibition of iNOS expression, by different agents, may depend on the inhibition of NF-kB activation. Besides, the role of NO in tumor onset and progression seems to be apparently paradoxical, since it can act as promoter or repressor, depending on the tumor microenvironment and type [34]. It is known that NF-kB is an important regulator in cell biology, but was also found to play a main role in pathological conditions, such as chronic inflammation, cancer and autoimmune diseases [35]. In humans, NF-kB family comprises five transcription factors, and the activation process is quite complex but well investigated; briefly, the inactive form resides within the cell cytoplasm until different signals trigger its activation and, consequently, its translocation into the nucleus, where it can regulate the expression of several genes responsible for inflammation, apoptosis, cell proliferation, angiogenesis, and so on [36]. However, more investigations are required, in order to gain more information about the modulation of NF-kB signaling, as it can be a crucial target for many diseases, including cancer and chronic inflammatory pathologies. The *status* of NF-kB under complexes **AuL9** or **AuL10** exposure was investigated in both RAW 264.7 and MDA.MB-231 cells, where they possessed the best activities, by the means of immunofluorescence assays. First, RAW 264.7 cells were stimulated with LPS (1 μg/mL) and, added with Ind, **AuL9** or **AuL10** (at a concentration of 5 μM, for 24 h). Control cells (CTRL) were added only with DMSO (vehicle). The results, shown in Figure 9, indicate a prominent cytoplasmatic localization of NF-kB in the vehicle-treated cells (Figure 9, panel 1B) and a net nuclear translocation under LPS treatment (Figure 9, panel 2B), as demonstrated by the superposition of the red (NF-kB) and blue (nucleus) fluorescences (Figure 9, panel 2C). The co-treatment LPS + Ind decreased the nuclear localization of NF-kB (Figure 9, panels 3B and C), as well as for the complexes **AuL9** or **AuL10**, meaning that both complexes were able to inhibit the NF-kB nuclear translocation (Figure 9, panels 4B and C, and 5B and C, respectively). These results are in agreement with the reduction of iNOS expression previously described.

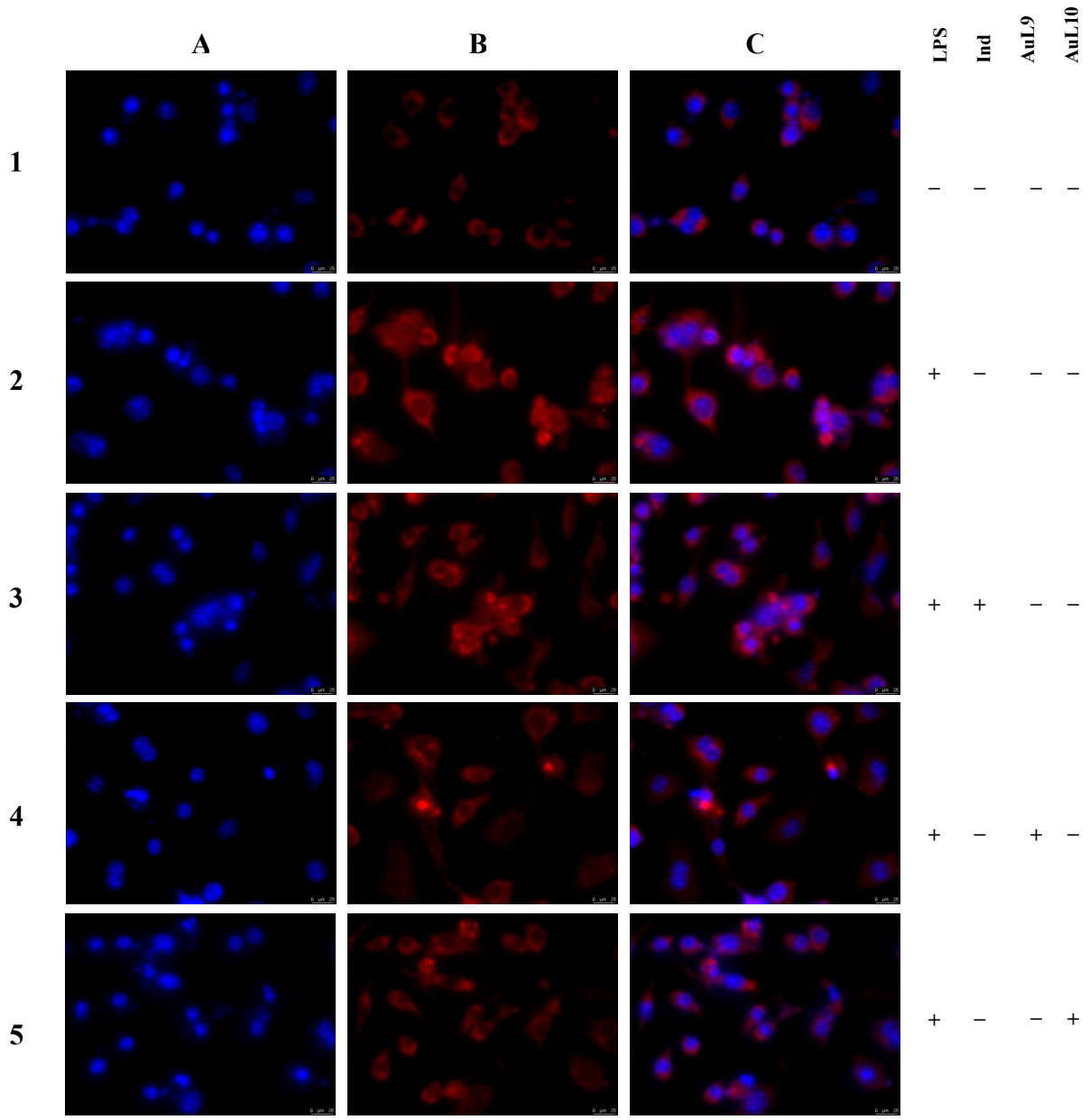

Figure 9. NF-kB localization in murine macrophages RAW 264.7. 1: vehicle (DMSO). 2: LPS (1 µg/mL). 3: LPS (1 µg/mL) + Ind. 4 and 5: LPS (1 µg/mL) + **AuL9** or **AuL10**, respectively. Panels A, DAPI (λex/em =350/460 nm); panels B, AlexaFluor®568 (λex/em = 644/665 nm); panels C, merge. Images acquired after 24 h of treatment (5 µM) at 40x. Representative fields of three different experiments are shown.

Next, a similar experiment was performed in MDA-MB-231 cells, for checking out whether NF-kB was also regulated in the adopted cancer cells context, using the same time of exposure and

compounds concentrations, as before. Figure 10 indicates that, under complexes **AuL9** or **AuL10** treatment, NF-kB (red fluorescence) is prevalently located in the cytoplasm, (panels B, **AuL9** and **AuL10**, respectively), and the nuclear area (blue fluorescence) is pretty uninterested. On the contrary, in the vehicle-treated cells NF-kB is present also into the nucleus (panel B, CTRL and panel C, merge), where its transcriptional activity is necessary for sustaining cancer growth and progression. Overall, both the complexes inhibited the activation of NF-kB and its translocation to the MDA-MB-231 cells' nucleus. Since NF-kB transcriptional activity in cancer cells is one of the main causes the inhibition of apoptosis [37], the found ability of the lead complexes in blocking NF-kB into the cytoplasm is another factor that contributes to the apoptosis induction, together with the above proved DNA damage caused by the inhibition of hTopoI.

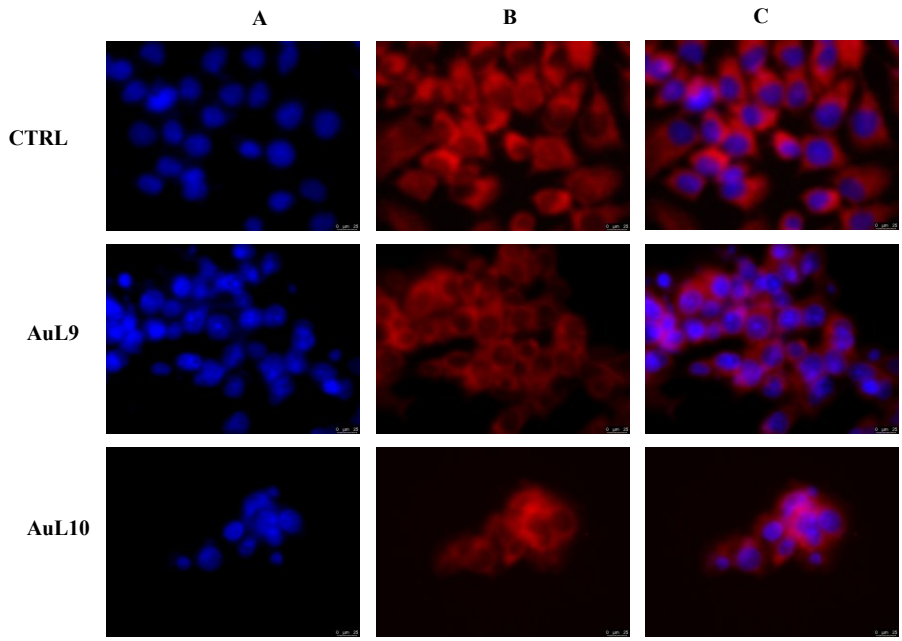

Figure 10. NF-kB localization in MDA-MB-231 cells exposed to DMSO (vehicle, CTRL), **AuL9** or **AuL10**, respectively. Panels A, DAPI (λex/em =350/460 nm); panels B, AlexaFluor®568 (λex/em = 644/665 nm); panels C, merge. Images were acquired at 40x, after 24 h of treatment (5 μM for **AuL9** or **AuL10**). Representative fields of three different experiments are shown.

2.6.Inhibition of TNFα production in MDA-MB-231 cells

NF-kB transcriptional activity is also responsible for the production of pro-inflammatory cytokines as TNFα, IL-1, IL-6 and so on [38]. Particularly, TNFα is considered a critical ad still debated player in cancer and inflammation, given that it may promote transformation, proliferation, angiogenesis, invasion ad that the constitutive production of TNFα from the microenvironment is a hallmark of several malignant tumors and is associated with a poor prognosis [39]. Moreover, TNFα can activate NF-kB *via* its receptor, TNF-R1, sustaining its pro-oncogenic and inflammatory activities, which are responsible for different aspects of oncogenesis [40]. For these reasons, the TNFα expression in MDA-MB-231 cells under the lead complexes exposure was determined. Cells were exposed for 24 h to vehicle (DMSO, CTRL), **AuL9** or **AuL10** (5 μM). Figure 11A indicates that under **AuL9** or **AuL10** there was a diminution of TNFα expression of around the 60% in both cases (panels B), if compared with the vehicle-treated cells (DMSO, panel B). Fluorescence quantification (Figure 11B) is also shown. This last aspect is very interesting, since the lead complexes reduce the TNFα production in the considered cancer cell context, influencing the loop existing between TNFα and NF-kB that are responsible for cancer onset, progression and inflammation burst.

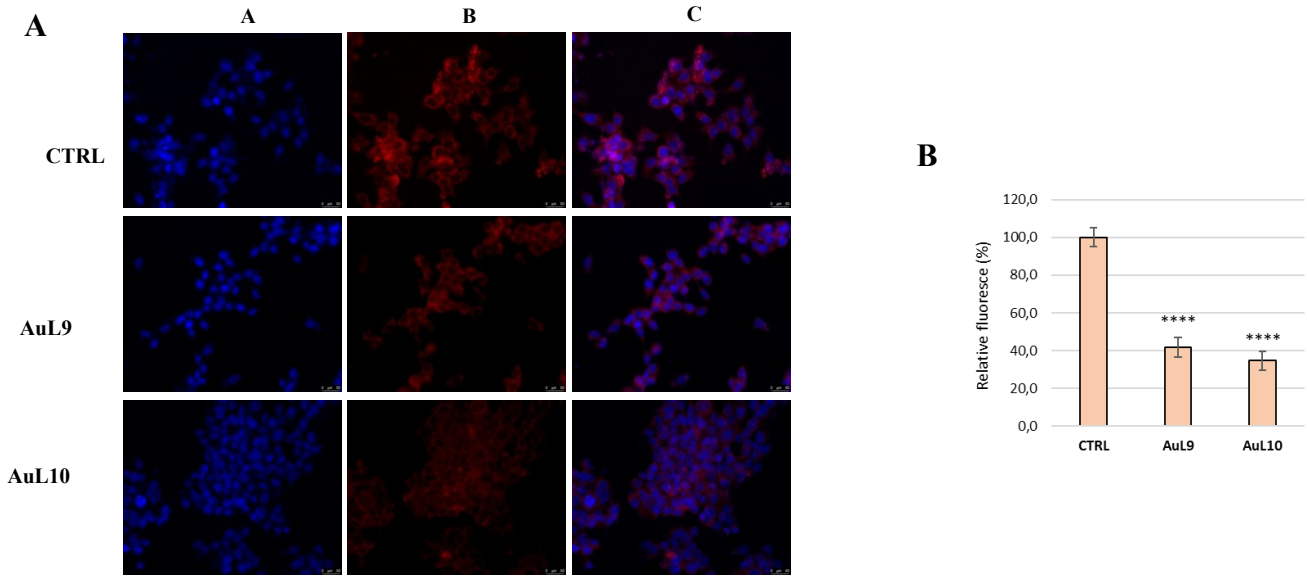

Figure 11. A) Semi-quantitative detection of TNFα expression. MDA-MB-231 cells were treated with DMSO (vehicle, CTRL), **AuL9** or **AuL10** at 5 μM, for 24 h. Panels A, DAPI ($\lambda_{ex}/_{em}$ =350/460 nm); panels B, AlexaFluor®568 ($\lambda_{ex}/_{em}$ = 644/665 nm); panels C, merge. Images were acquired at 20x

and represent three different experiments. B) ImageJ software was used for fluorescence quantification; **AuL9** and **AuL10** *vs* CTRL, ****p<0.0001.

Summing up, the individuated leads exerted their anticancer and anti-inflammatory properties regulating the activation of NF-kB in the two cellular contests considered, an aspect that is very important for facing the cancer progression and the associated excessive inflammation that causes further tissue damage.

2.7.Antioxidant activity in murine fibroblasts BALB/3T3

Several carbazole-based compounds, both natural and synthetic, were proved to possess different pharmacological activities, particularly anticancer, anti-inflammatory and antioxidant [6, 9, 15, 18, 41]. Besides, NHC-Au complexes properties were largely discussed and partially overlap those from carbazole derivatives [5, 8, 10, 11, 13, 18, 24, 42]. Considered that the lead complexes hold interesting anticancer and anti-inflammatory properties, and that the exacerbation of the intracellular oxidative stress was proved to be one of the leading causes of various diseases, included cancer [43], we tested the synthetized hybrid complexes for their potential ROS scavenging activity. At this purpose, a cell-based test, employing the dihydro-2',7'-dichlorofluorescein diacetate (H_2DCF-DA) fluorescent probe, was performed in murine fibroblasts BALB/3T3. In this established and very adopted cell model, the ROS production was stimulated using menadione (Men, 25 μM, 15 minutes), after a pre-incubation with all the complexes at 5 and 10 μM for 24 hours. As reference molecule, N-acetyl-cysteine (NAC), which is a potent antioxidant, was used as positive control, at 20 mM concentration. The lack of cytotoxicity of the adopted treatments was previously ascertained by MTT assays under the same experimental conditions, producing about the 95% of residual viability *versus* the vehicle-treated cells (data not shown). Figure 12 shows the obtained outcomes, where it is possible to notice that the best antioxidant complexes were **AuL8**, **AuL9** and **AuL10**, in a dose-dependent manner. In details, complex **AuL8** and **AuL9** reduced the ROS production with very close percentage values, being of about 62% and 81-82% at 5 and 10 μM, respectively. Complex **AuL10** was the most active, with a ROS diminution of about 72 and 86%, at 5 and 10 μM, respectively. These activities are very exciting, considering that NAC, at the concentration of 20 mM, was able to scavenge the ROS of about 91%. The latter results make the hybrid complexes very promising as anticancer and anti-inflammatory compounds, since they were found also able to strongly reduce the intracellular induced oxidative stress that is a well-established cause of cancer and inflammatory diseases.

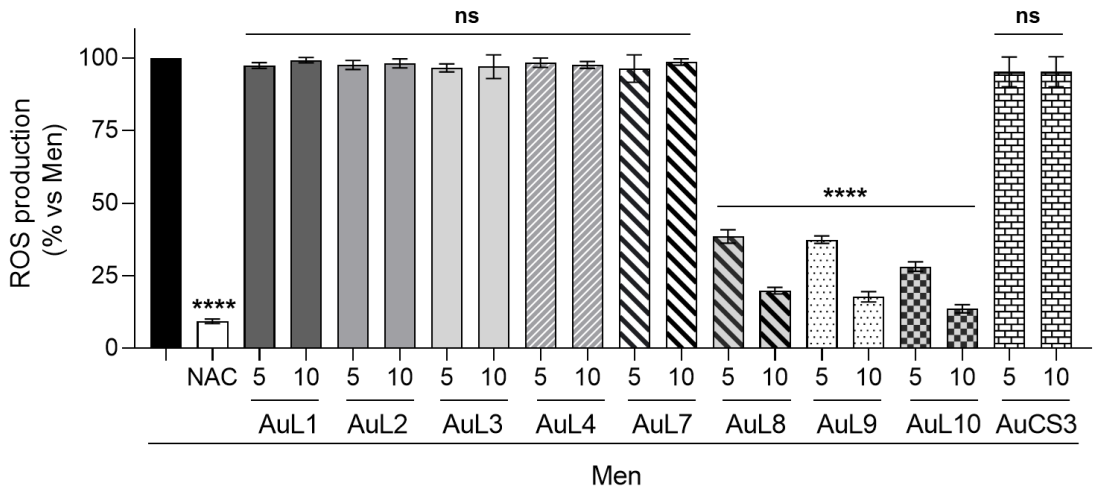

Figure 12. ROS scavenging activity determined *in vitro* on murine fibroblasts BALB/3T3. Cells were preincubated with the complexes or NAC for 24 h, at the indicated concentrations. ROS production was obtained treating with Men (25 μM, 15 minutes). ****p<0.0001, *ns* not significant, NAC or **AuL1-10** and **AuCS3** *vs* only Men.

3.Conclusions

The need of new compounds in cancer therapy is still an urgent issue, nevertheless the great progresses in this field. The poly-pharmacologic approach toward cancer and other related diseases, which are more complex and multi-factorial, represents a winning strategy. Indeed, a drug able to targets different proteins and pathways involved in cancer onset and development is often more effective than a single target drug. The design and synthesis of hybrid molecules, with a multitarget effectiveness, attracted the interests of many scientists during the last few decades. The possibility of a fine tuning for obtaining new chimeric compounds could also improve the wanted effects and avoid the so-called off-target adverse effects. Under this perspective, herein we reported the design and synthesis of new hybrid molecules, composed by NHC-Au(I) complexes and *N*-alkylthiolated carbazoles moieties, and evaluated their biological effects by *in silico* and *in vitro* assays. Our outcomes indicated that the individuated leads possess good features, as anticancer, anti-inflammatory and antioxidant agents, combined together. Particularly, they were found able to induce cancer cells death *via* the hTopoI inhibition and genomic DNA damage, regulate the NF-kB transcriptional activity and decrease the TNFα intracellular production. Furthermore, these complexes

also inhibited the iNOS activity and diminished its expression in RAW 264.7 murine macrophages, regulating, as well in this cell context, the NF-kB transcriptional activity. Finally, they also acted as good ROS scavengers in BALB/3T3 murine fibroblasts, under oxidative stress induction. The ability to regulate the individuated intracellular targets responsible for cancer onset and progression make them valid candidates for further studies and for the improvement of a multitarget drug approach.

4.Materials and Methods

4.1.Chemistry

All reagents and solvents were purchased from Sigma-Aldrich and TCI Chemicals. Reaction with Au-precursor were carried out under an oxygen and moisture-free atmosphere using Schlenk techniques. Glassware used were dried in an oven at 120 °C overnight. Methylene chloride (CH_2Cl_2) and acetonitrile were distilled under nitrogen over CaH_2. Organic molecules were purified through flash column chromatography using silica gel 60 (230–400 mesh) purchased from Merck Italy. Thin-layer chromatography (TLC) was performed using silica gel 60 aluminum foils with an F254 fluorescence indicator. Deuterated solvents were dried over molecular sieves. ^{1}H and ^{13}C nuclear magnetic resonance spectra (NMR) were acquired on a Bruker Avance 250 spectrometer (250 MHz for ^{1}H; 62.5 MHz for ^{13}C) and a Bruker AVANCE 400 spectrometer (400 MHz for ^{1}H; 100 MHz for ^{13}C) operating at 298 K. NMR samples were prepared by dissolving about 15-20 mg of compound in 0.5 mL of deuterated solvent. The chemical shifts of ^{1}H-NMR and ^{13}C-NMR spectra are referenced using the residual proton impurities of the deuterated solvents as internal standards. ^{1}H NMR spectra are referenced using the residual solvent peak δ 2.50 for DMSO-d_6 and δ 7.27 for $CDCl_3$. ^{13}C NMR spectra are referenced using the residual solvent peak at δ 39.51 for DMSO-d_6 and δ 77.23 for $CDCl_3$. The spectra multiplicities are indicated as follows: singlet (s), doublet (d), triplet (t), multiplet (m), broad (br) and overlapped (o). Elemental analysis was conducted with a PERKIN-Elmer 240-C analyzer. MALDI-MS mass spectra were achieved by Bruker SolariX XR Fourier transform ion cyclotron resonance mass spectrometer (Bruker Daltonik GmbH, Bremen, Germany) with a 7 T refrigerated actively shielded superconducting magnet (Bruker Biospin, Wissembourg, France). MALDI ion source (Bruker Daltonik GmbH, Bremen, Germany) was used the samples in positive ion mode. The mass range was set to m/z 200–3000. The laser power was 28% and 22 laser shots were utilized for each scan. The mass spectra were calibrated externally using a mix of peptide clusters in MALDI ionization positive ion mode. A linear calibration was applied.

6-bromo-9-(8-bromooctyl)-1,4-dimethyl-9H-carbazole (**C4**), 6-bromo-9-(9-bromononyl)-1,4-dimethyl-9H-carbazole (**C5**), 7-(6-bromo-1,4-dimethyl-9H-carbazol-9-yl)-heptane-1-thiol (**CS3**), 8-(6-bromo-1,4-dimethyl-9H-carbazol-9-yl)-octane-1-thiol (**CS4**), 9-(6-bromo-1,4-dimethyl-9H-carbazol-9-yl)-nonane-1-thiol (**CS5**) were synthesized according to procedures detailed in the literature [6, 44]. N-methyl, N'-[(2-hydoxy-2-phenyl)ethyl]imidazolium iodide (**L5**), N-methyl, N'-[(2-hydoxy-2-phenyl)ethyl]-4,5-dichloroimidazolium iodide (**L6**), (N-methyl-N'-(2-hydroxy-2-phenyl)ethyl-imidazole-2-ylidene]gold(I) chloride (**AuL5**), (N-methyl-N'-(2-hydroxy-2-

phenyl)ethyl-4,5-dichloroimidazole-2-ylidene]gold(I) chloride (**AuL6**) were obtained following procedures outlined in the literature [17, 18, 25].

Synthesis of 6-bromo-9-(2-bromoethyl)-1,4-dimethyl-9H-carbazole (C2)

At a suspension of potassium hydroxide (KOH, 1.02 g, 18.24 mmol, 5.00 eq), potassium carbonate (K_2CO_3, 3.03 g, 21.90 mmol, 6.00 eq), tetrabutylammonium bromide (TBAB, 0.0258 g, 0.08 mmol, 0.02 eq) and 1,2-dibromoethane (2.06 g, 0.94 mL, 10.95 mmol, 3.00 eq), **C1** (1.00 g, 3.65 mmol, 1.00 eq) was added. The reaction mixture was heated to 60 °C overnight. Following this, the reaction mixture was filtered off, diluted with CH_2Cl_2, extracted with water for three times (3x50 mL) and dehydrated using before Na_2SO_4 and after $MgSO_4$. The mixture has been filtered and the solvent removed by evaporation. The crude product was purified by column chromatography on silica gel (petroleum ether: dichloromethane 2:1) to give the desired product as a white powder. Yield 45%.

^{1}H-NMR (ppm, $CDCl_3$, 400 MHz): δ 8.28 (s, 1H, aromatic hydrogen), 7.57 (d, *J* 8 Hz, 1H, aromatic hydrogen), 7.33 (d, *J* 8 Hz, 1H, aromatic hydrogen), 7.14 (d, *J* 8 Hz, 1H, aromatic hydrogen), 6.96 (d, *J* 8 Hz, 1H, aromatic hydrogen), 4.89 (t, *J* 16 Hz, 2H, NC***H*₂**), 3.56 (t, *J* 16 Hz, 2H, C***H*₂**Br), 2.82 (s, 3H, Ar-C***H*₃**), 2.79 (s, 3H, Ar-C***H*₃**).

^{13}C-NMR (ppm, $CDCl_3$, 62.5 MHz): δ 139.06, 138.65, 131.74, 129.89, 127.88, 125.72, 125.29, 121.86, 121.48, 117.30, 112.51, 109.65 (aromatic carbons), 46.08 (N***C***H_2), 28.18 (***C***H_2Br), 20.80 (Ar-***C***H_3), 19.90 (Ar-***C***H_3).

Maldi-MS ($CHCl_3$) calcd/found (m/z): $[C_{16}H_{15}Br_2N]^+$ 380.95459/380.95572. Elemental Analysis: Calculated for $C_{16}H_{15}Br_2N$ (381.11) C, 50.43; H, 3.97; N, 3.68. Found C, 50.40; H, 3.93; N, 3.69.

General Procedure for Synthesis of N-Heterocyclic carbene proligands (L1-4)

Imidazolium salts **L1**, **L2**, **L3** and **L4** were synthesized following the general procedure reported below.

Imidazole or 4,5-dichloroimidazole (1.0 eq), phenylethylene oxide (1.2 eq) and dry acetonitrile (0.02 M) were introduced in a round-bottomed flask equipped with a magnetic stirrer. The reaction mixture was stirred at reflux for 12h, then filtered and the solvents removed to give *N*-monoalkylated products (**P1** and **P2**) as a white powder. Yields: **P1**, 74%; **P2**, 49%.

P1 – *(N-(2-phenyl-2-hydroxyethyl))-imidazole*

^{1}H-NMR (ppm, DMSO-d_6, 400 MHz): δ 7.49 (s, 1H, N=C***H***N), 7.34–7.33 (m, 5H, aromatic hydrogens), 7.12 and 6.18 (s, 2H, NC***H***C***H***N), 5.74 (br, 1H, CHO***H***), 4.81 (m, 1H, NCH_2C***H***OH), 4.12-4.03 (dd, *J* 4 Hz, *J* 28 Hz, 2H, NC$\boldsymbol{H_2}$CH).

^{13}C-NMR (ppm, DMSO-d_6, 75 MHz): δ 142.64 (ipso carbon of aromatic ring), 137.69 (N=***C***HN), 128.05, 127.71, 127.31, 126.00, 120.01 (aromatic carbons and N***C***H***C***HN), 72.07 (***C***HOH), 53.53 (N***C***H_2CH).

P2 – *(N-(2-phenyl-2-hydroxyethyl))-4,5-dichloro-imidazole*

^{1}H-NMR (ppm, DMSO-d_6, 400 MHz): δ 7.69 (s, 1H, N=C***H***N), 7.34 (m, 5H, aromatic hydrogens), 5.84 (br, 1H, CHO***H***), 4.86-4.82 (m, 1H, NCH_2C***H***OH), 4.10-4.06 (m, 2H, NC$\boldsymbol{H_2}$CH).

^{13}C-NMR (ppm, DMSO-d_6, 75 MHz): δ 141.73 (ipso carbon of aromatic ring), 136.71 (N=***C***HN), 128.85, 128.26, 127.67, 126.84, 125.92 (aromatic carbons) 123.78 and 112.41 (N***C***Cl***C***ClN), 70.77 (***C***HOH), 52.71 (N***C***H_2CH).

Afterwards, in a solution of **P1** or **P2** (1.00 eq) and dry acetonitrile (0.05 M) was added **C2** or **C3** (1.00 eq). The mixtures were stirred for 48 hours at 80 °C. After filtration on a celite plug, the solvent was removed under reduced pressure and the imidazolium salts **L1** (41%), **L2** (31%), **L3** (39%) and **L4** (38%) were obtained as a white solid.

L1 - *3-(2-(6-bromo-1,4-dimethyl-9H-carbazol-9-yl)ethyl)-1-(2-hydroxy-2-phenylethyl)-1H-imidazol-3-ium bromide*

^{1}H-NMR (ppm, DMSO-d_6, 300 MHz): δ 9.00 (s, 1H, NC***H***N), 8.21 (s, 1H, aromatic hydrogen), 7.72 -6.96 (m, 11H, aromatic hydrogens + NC***H***C***H***N), 6.00 (d, *J* 3 Hz, 1H, O***H***), 5.00 (m, 2H, NC$\boldsymbol{H_2}$$CH_2$N), 4.78 (m, 1H, C***H***OH), 4.65 (m, 2H, NCH_2C$\boldsymbol{H_2}$N), 4.27 (dd, *J* 9 Hz, *J* 42 Hz, 2H, NC$\boldsymbol{H_2}$CHOH), 2.76 (s, 3H, Ar-C$\boldsymbol{H_3}$), 2.72 (s, 3H, Ar-C$\boldsymbol{H_3}$).

^{13}C-NMR (ppm, DMSO-d_6, 100 MHz): δ 141.19, 139.32, 138.51, 136.96, 130.96, 129.91, 128.34, 127.85, 127.45, 125,98, 124.74, 124.27, 123.21, 122.54, 121.71, 121.46, 120.77, 118.77 (aromatic carbons), 111.67, 110.76 (N***C***H***C***HN), 70.74 (***C***HOH), 55.53 (N***C***H_2CHOH), 48.56 (N***C***H_2), 44.17 (N***C***H_2), 20.42 (Ar-***C***H_3), 19.70 (Ar-***C***H_3).

Maldi-MS (CH_3CN) calcd/found (m/z): $[C_{27}H_{29}BrN_3O]^+$ 490.13154/490.13093. Elemental Analysis: Calculated for $C_{27}H_{27}Br_2N_3O$ (569.34) C, 56.96; H, 4.78; N, 7.38. Found C, 56.96; H, 4.79; N, 7.36.

L2 - *3-(2-(6-bromo-1,4-dimethyl-9H-carbazol-9-yl)ethyl)-4,5-dichloro-1-(2-hydroxy-2-phenylethyl)-1H-imidazol-3-ium bromide*

^{1}H-NMR (ppm, $CDCl_3$, 400 MHz): δ 8.28 (s, 1H, NC***H***N), 7.58–6.95 (m, 10H, aromatic hydrogens), 5.03 (d, *J* 3 Hz, 1H, C***H***OH), 4.88 (t, *J* 16 Hz, 2H, NC***H₂***CH_2N), 4.14 (dd, *J* 16 Hz, *J* 48 Hz, 2H, NC***H₂***CHOH), 3.56 (t, *J* 16 Hz, 2H, NCH_2C***H₂***N), 2.82 (s, 3H, Ar-C***H₃***), 2.78 (s, 3H, Ar-C***H₃***).

^{13}C-NMR (ppm, $CDCl_3$, 100 MHz): δ 139.58, 138.66, 138.23, 135.15, 131.29, 128.42, 128.10, 127.44, 125.28, 124.48, 128.10, 127.44, 125.28, 127.44, 125.28, 124.85, 121.42, 121.05, 116.87, 112.95, 112.07, 109.23 (aromatic carbons and N***C***Cl***C***ClN), 71.37 (***C***HOH), 53.25 (N***C***H_2CHOH), 45.66 (N***C***H_2), 27.66 (N***C***H_2), 20.33 (Ar-***C***H_3), 19.43 (Ar-***C***H_3).

Maldi-MS (CH_3CN) calcd/found (m/z): $[C_{27}H_{27}BrCl_2N_3O]^+$ 558.05310/558.05124. Elemental Analysis: Calculated for $C_{27}H_{25}Br_2Cl_2N_3O$ (638.22) C, 50.81; H, 3.95; N, 6.58. Found C, 50.80; H, 3.96; N, 6.56.

L3 - *3-(7-(6-bromo-1,4-dimethyl-9H-carbazol-9-yl)heptyl)-1-(2-hydroxy-2-phenylethyl)-1H-imidazol-3-ium bromide*

^{1}H-NMR (ppm, $CDCl_3$, 400 MHz): δ 9.66 (s, 1H, NC***H***N), 8.25 (s, 1H, aromatic hydrogen), 7.53–6.89 (m, 11H, aromatic hydrogens and NC***H***C***H***N), 5.25 (d, *J* 3 Hz, 1H, O***H***), 4.67 (br d, 1H, C***H***OH), 4.45 (t, *J* 16 Hz, 2H, NC***H₂***CH_2), 4.35 (m, 2H, NC***H₂***CH), 4.05 (t, *J* 16 Hz, 2H, NCHNC***H₂***), 2.79 (s, 3H, Ar-C***H₃***), 2.75 (s, 3H, Ar-C***H₃***), 1.74-1.16 (m, 10H, (C***H₂***)$_5$).

^{13}C-NMR (ppm, $CDCl_3$, 75 MHz): δ 139.33, 139.17, 138.69, 136.39, 131.05, 129.05, 128.16, 127.57, 127.03, 125.64, 124.96, 124.61, 123.00, 120.65, 120.37, 117.16, 117.07, 111.16, 109.82, 109.54 (aromatic carbons and N***C***H***C***HN), 70.38 (***C***HOH), 56.25 (N***C***H_2CH), 49.48 (N***C***H_2CH_2), 44.39 (NCHNC***H₂***), 30.03, 28.10, 27.57, 26.32, 25.54 (***C***H_2 of alkyl chain), 20.39 (Ar-***C***H_3), 19.67 (Ar-***C***H_3).

Maldi-MS (CH_3CN) calcd/found (m/z): $[C_{32}H_{38}BrN_3O]^+$ 560.20993/560.21102. Elemental Analysis: Calculated for $C_{30}H_{33}Br_2N_3O$ (611.42) C, 58.93; H, 5.44; N, 6.87. Found C, 58.95; H, 5.42; N, 6.88.

L4 - *3-(7-(6-bromo-1,4-dimethyl-9H-carbazol-9-yl)heptyl)-4,5-dichloro-1-(2-hydroxy-2-phenylethyl)-1H-imidazol-3-ium bromide*

^{1}H-NMR (ppm, $CDCl_3$, 400 MHz): δ 10.68 (s, 1H, NC***H***N), 8.26 (s, 1H, aromatic hydrogen), 7.52–6.90 (m, 9H, aromatic hydrogens), 5.63 (s, *J* 3 Hz, 1H, O***H***), 5.28 (t, *J* 4 Hz, 1H, C***H***OH), 4.62-4.53 (m, 4H, NC***H₂***CH + N***C***H_2), 4.20 (m, 2H, NC***H₂***), 2.81 (s, 3H, Ar-C***H₃***), 2.77 (s, 3H, Ar-C***H₃***), 1.87-1.22 (m, 10H, (C***H₂***)$_5$).

^{13}C-NMR (ppm, $CDCl_3$, 75 MHz): δ 139.18, 138.83, 138.68, 137.24, 131.01, 129.05, 128.29, 127.90, 127,08, 125.73, 124.90, 124.54, 120.75, 120.63, 119.07, 118.18, 117.15, 11.14, 109.80 (aromatic

carbons and N***C***Cl***C***ClN), 69.79 (***C***HOH), 54.54 (N***C***H_2CH), 48.81 (N***C***H_2), 44.31 (N***C***H_2), 30.07, 28.44, 28.18, 26.14, 25.44 (***C***H_2 of alkyl chain), 20.42 (Ar-***C***H_3), 19.76 (Ar-***C***H_3).

Maldi-MS (CH_3CN) calcd/found (m/z): $[C_{32}H_{35}BrCl_2N_3O]^+$ 628.13144/628.13090. Elemental Analysis: calculated for $C_{30}H_{31}Br_2Cl_2N_3O$ (680.30) C, 52.97; H, 4.59; N, 6.18. Found C, 52.96; H, 4.61; N, 6.17.

General procedure for synthesis of gold(I) complexes AuL1-4

In a round bottom flask, equipped by magnetic stirrer and a condenser, the imidazolium salt (**L1**, **L2**, **L3** or **L4**, 1.00 eq) was dissolved in dry dichloromethane (0.02 M) and chloro(dimethylsulfide)gold(I) (1.00 eq) was added. The reaction mixture was stirred for 24 h at room temperature. After that, the mixture was filtered on celite, and the solution was dried under reduced pressure. Washings with hexane (3x10 mL) gave a yellow amorphous powder. Yields: **AuL1** 40%, **AuL2** 30%, **AuL3** 58%, **AuL4** 80%.

AuL1 - *(3-(2-(6-bromo-1,4-dimethyl-9H-carbazol-9-yl)ethyl)-1-(2-hydroxy-2-phenylethyl)-1H-imidazol-2-yl)gold(I) chloride*

^{1}H-NMR (ppm, $CDCl_3$, 300 MHz): δ 8.30 (s, 1H, aromatic hydrogen), 7.60–6.92 (o, 11H, aromatic hydrogens), 5.06-4.88 (o, 3H, C***H***OH and NC***H₂***), 4.51 (m, 2H, NC***H₂***CH), 3.57 (t, *J* 9 Hz, 2H, NC***H₂***), 2.83 (s, 3H, Ar-C***H₃***), 2.80 (s, 3H, Ar-C***H₃***).

^{13}C-NMR (ppm, $CDCl_3$, 75 MHz): δ 199.79 (N***C***N), 139.75, 139.02, 138.67, 138.25, 131.30, 129.47, 128.41, 128.33, 128.02, 127.46, 125.43, 125.16, 124.87, 124.67, 121.68, 121.43, 121.06, 120.02, 119.50, 116.90, 112.08, 109.58, 109.27 (aromatic carbons and N***C***H***C***HN), 73.23 (***C***HOH), 57.98 (N***C***H_2CH), 45.68, 27.70 (***C***H_2 of alkyl chain), 20.36 (Ar-***C***H_3), 19.47 (Ar-***C***H_3).

Maldi-MS (CH_3CN) found (*m/z*): $[C_{38}H_{39}AuBrN_5O_2]^+$ 874.22231 Dalton. Elemental Analysis: calculated for $C_{27}H_{26}AuBrClN_3O$ (720.84) C, 44.99; H, 3.64; N, 5.83. Found C, 44.98; H, 3.63; N, 5.84.

AuL2 - *((3-(2-(6-bromo-1,4-dimethyl-9H-carbazol-9-yl)ethyl)-4,5-dichloro-1-(2-hydroxy-2-phenylethyl)-1H-imidazol-2-yl)gold(I) chloride*

^{1}H-NMR (ppm, $CDCl_3$, 400 MHz): δ 8.27 (s, 1H, aromatic hydrogen), 7.56–6.94 (o, 9H, aromatic hydrogens), 5.00 (m, *J* 4 Hz, 1H, C***H***OH), 4.88 (t, *J* 4 Hz, 2H, NC***H₂***), 4.12 (dd, *J* 4 Hz, *J* 8 Hz, 2H, NC***H₂***CH), 3.55 (t, *J* 4 Hz, 2H, NC***H₂***), 2.81 (s, 3H, Ar-C***H₃***), 2.77 (s, 3H, Ar-C***H₃***).

^{13}C-NMR (ppm, $CDCl_3$, 150 MHz): δ 204.44 (N***C***N), 140.71, 139.85, 139.43, 136.32, 132.48, 130.63, 193.90, 129.65, 129.41, 128.64, 126.50, 126.46, 126.36, 126.05, 122.60, 122.25, 118.06, 113.26, 110.43 (aromatic carbons and N***C***Cl***C***ClN), 72.86 (***C***HOH), 54.17 (N***C***H_2CH), 46.86 (NC***H₂***), 28.84 (N***C***H_2), 21.52 (Ar-***C***H_3), 20.63 (Ar-***C***H_3).

Maldi-MS (CH_3CN) found (m/z): $[C_{54}H_{47}AuBr_2Cl_4N_6O]^+$ 1293.52602 Dalton. Elemental Analysis: calculated for $C_{27}H_{24}AuBrCl_3N_3O$ (789.72) C, 41.06; H, 3.06; N, 5.32. Found C, 41.05; H, 3.04; N, 5.33.

AuL3 - *(3-(7-(6-bromo-1,4-dimethyl-9H-carbazol-9-yl)heptyl)-1-(2-hydroxy-2-phenylethyl)-1H-imidazol-2-yl)gold(I) chloride*

^{1}H-NMR (ppm, $CDCl_3$, 400 MHz): δ 8.25 (s, 1H, aromatic hydrogen), 7.53–6.81 (o, 11H, aromatic hydrogens), 5.24 (br, m, 1H, C***H***OH), 4.48 (br, m, 2H, NC***H₂***), 4.12 (o, 4H, NC***H₂***CH and NC***H₂***), 2.78 (s, 3H, Ar-C***H₃***), 2.77 (s, 3H, Ar-C***H₃***), 1.78 and 1.37 (o, 10H, (C***H₂***)$_5$).

^{13}C-NMR (ppm, $CDCl_3$, 100 MHz): 173.49 (N***C***N), 139.14, 138.67, 130.97, 129.03, 128.32, 127.88, 127.30, 127.01, 125.74, 125.45, 124.88, 124.60, 124.53, 122.05, 120.68, 120.61, 119.05, 117.16, 117.06, 111.11, 109.74, 109.53 (aromatic carbons and N***C***H***C***HN), 73.33 (***C***HOH), 57.66 (N***C***H_2CH), 50.57 (N***C***H_2), 44.37 (N***C***H_2), 30.08, 28.08, 27.55, 26.30, 25.54 (***C***H_2 of alkyl chain), 20.38 (Ar-***C***H_3), 19.67 (Ar-***C***H_3).

Maldi-MS (CH_3CN) calcd/found (m/z): $[C_{32}H_{38}AuBrN_3O]^+$ 757.17650/757.17181. Elemental Analysis: calculated for $C_{30}H_{32}AuBrClN_3O$ C, 47.23; H, 4.23; N, 5.51. Found C, 47.25; H, 4.21; N, 5.51.

AuL4 - *(3-(7-(6-bromo-1,4-dimethyl-9H-carbazol-9-yl)heptyl)-4,5-dichloro-1-(2-hydroxy-2-phenylethyl)-1H-imidazol-2-yl)gold(I) chloride*

^{1}H-NMR (ppm, $CDCl_3$, 400 MHz): δ 8.23 (s, 1H, aromatic hydrogen), 7.53–6.87 (o, 9H, aromatic hydrogens), 5.37 (m, 1H, C***H***OH), 4.48 (t, *J* 8 Hz, 2H, NC***H₂***), 4.28 (d, *J* 8 Hz, NC***H₂***CH), 4.14 (t, *J* 8 Hz, 2H, NC***H₂***), 2.78 (s, 3H, Ar-C***H₃***), 2.76 (s, 3H, Ar-C***H₃***), 1.77 and 1.36 (o, 10H, (C***H₂***)$_5$).

^{13}C-NMR (ppm, $CDCl_3$, 100 MHz): δ 175.05 (N***C***N), 139.69, 139.66, 139.17, 131.51, 129.56, 129.01, 128.80, 127.60, 125.97, 125.38, 125.06, 121.23, 121.12, 118.08, 117.68, 116.62, 111.66, 110.30 (aromatic carbons and N***C***Cl***C***ClN), 73.62 (***C***HOH), 56.52 (N***C***H_2CH), 50.40 (N***C***H_2), 44.88 (N***C***H_2), 30.62, 30.01, 28.78, 26.71, 26.02 (***C***H_2 of alkyl chain), 20.96 (Ar-***C***H_3), 20.32 (Ar-***C***H_3).

Maldi-MS (CH_3CN) calcd/found (m/z): $[C_{32}H_{35}AuBrCl_3N_3O]^+$ 859.0613/859.0721. Elemental Analysis: calculated for $C_{30}H_{30}AuBrCl_3N_3O$ (831.81) C, 43.32; H, 3.64; N, 5.05. Found C, 43.32; H, 3.63; N, 5.06.

General procedure for the synthesis of *N*-heterocyclic carbene *N*-thioalkyl carbazole gold(I) complexes (AuL7-AuL10)

The reaction was conducted in nitrogen atmosphere. *N*-thioalkylcarbazole (1.00 eq, **CS3**-**CS5**), triethylamine ($N(CH_2CH_3)_3$, 1.00 eq), and dry dichloromethane (0.02 M) were introduced into a two-necked flask equipped with a magnetic stirrer. After 15 minutes, the gold complex stabilized by the N-heterocyclic carbenic ligand (**AuL5** or **AuL6**) was added to the mixture. The reaction was stirred, under a nitrogen flow, for 4 hours at room temperature in the dark. After that, the solvent was removed under reduced pressure, followed by solubilization in the minimal amount of THF, and filtration on celite. The eluted was then concentrated and a brownish solid was obtained by washing with hexane (3 x 10 mL). Yields: **AuL7** 40%, **AuL8** 33%, **AuL9** 88%, **AuL10** 77%.

AuL7 - *((7-(6-bromo-1,4-dimethyl-9H-carbazol-9-yl)heptyl)thio)(1-(2-hydroxy-2-phenylethyl)-3-methyl-1H-imidazol-2-yl)gold*

^{1}H-NMR (ppm, $CDCl_3$, 300 MHz): δ 8.17 (s, 1H, aromatic hydrogen), 7.44 - 6.75 (o, 11H, aromatic hydrogens), 5.10 (m, 1H, C***H***OH), 4.40 (o, 4H, NC***H₂*** and NC***H₂***CH), 3.72 (s, 3H, NC***H₃***), 2.71 (s, 3H, Ar-C***H₃***), 2.67 (s, 3H, Ar-C***H₃***), 2.54 (t, *J* 8 Hz, 2H, C***H₂***SAu) 1.68-1.126 (o, 10H, (C***H₂***)$_5$).

^{13}C-NMR (ppm, $CDCl_3$, 100 MHz): δ 170.88 (N***C***N), 141.14, 140.60, 139.64, 139.17, 131.53, 129.51, 128.77, 128.66, 128.55, 128.30, 128.06, 127.90, 127.50, 126.31, 126.03, 125.42, 125.08, 123.13, 122.70, 121.73, 121.24, 121.10, 117.56, 111.62, 110.04 (aromatic carbons and N***C***H***C***HN), 73.75 (***C***HOH), 58.27 (N***C***H_2CH), 45.92 (N***C***H_2), 44.90 (S***C***H_2), 38.91 (N***C***H_3), 38.27, 30.52, 29.01, 28.32, 26.81 (***C***H_2 of alkyl chain), 20.87 (Ar-***C***H_3) 20.15 (Ar-***C***H_3).

Maldi-MS (CH_3CN) calcd/found (m/z): $[C_{33}H_{40}AuBrN_3NaOS]^+$ 827.1790/827.1668. Elemental Analysis: calculated for $C_{31}H_{36}AuBrN_3OS$ (775.58) C, 48.01; H, 4.68; N, 5.42. Found C, 48.03; H, 4.66; N, 5.41.

AuL8 - *((7-(6-bromo-1,4-dimethyl-9H-carbazol-9-yl)heptyl)thio)(4,5-dichloro-1-(2-hydroxy-2-phenylethyl)-3-methyl-1H-imidazol-2-yl)gold*

^{1}H-NMR (ppm, $CDCl_3$, 300 MHz): δ 8.24 (s, 1H, aromatic hydrogen), 7.52 - 6.88 (o, 9H, aromatic hydrogens), 5.38 (m, 1H, C***H***OH), 4.44 (m, 2H, NC***H₂***,), 4.27 (br d, 2H, NC***H₂***CH), 3.79 (s, 3H,

NC***H₃***), 2.79 (s, 3H, Ar-C***H₃***), 2.76 (s, 3H, Ar-C***H₃***), 2.63 (t, *J* 9 Hz, 2H, C***H₂***SAu) 1.76-1.38 (o, 10H, (C***H₂***)$_5$).

^{13}C-NMR (ppm, $CDCl_3$, 75 MHz): δ 171.86 (N***C***N), 140.17, 139.66, 139.20, 131.57, 129.59, 128.92, 128.57, 127.56, 126.01, 125.48, 125.11, 121.16, 118.20, 117.65, 117.34, 111.68, 110.15 (aromatic carbons and N***C***Cl***C***ClN), 73.39 (***C***HOH), 56.76 (N***C***H_2CH), 45.94 (N***C***H_2), 44.97 (S***C***H_2), 38.96 (N***C***H_3), 37.23, 30.64, 29.09, 28.41, 26.89 (***C***H_2 of alkyl chain), 20.99 (Ar-***C***H_3) 20.26 (Ar-***C***H_3).

ESI-MS (CH_3CN) found (m/z): $[C_{33}H_{36}ClON_3AuS]^+$ 739.01 Dalton. Elemental Analysis: calculated for $C_{31}H_{34}AuBrCl_2N_3OS$ (844.46) C, 44.09; H, 4.06; N, 4.98. Found C, 44.10; H, 4.06; N, 4.99.

AuL9 - *((8-(6-bromo-1,4-dimethyl-9H-carbazol-9-yl)octyl)thio)(4,5-dichloro-1-(2-hydroxy-2-phenylethyl)-3-methyl-1H-imidazol-2-yl)gold*

^{1}H-NMR (ppm, $CDCl_3$, 250 MHz): δ 8.26 (s, 1H, aromatic hydrogen), 7.35-6.91 (o, 9H, aromatic hydrogens), 5.37 (m, 1H, C***H***OH), 4.44 (m, 2H, NC***H₂***), 4.30 (br d, 2H, NC***H₂***CH), 3.82 (s, 3H, NC***H₃***), 2.80-2.76 (o, 8H, Ar-C***H₃***, Ar-C***H₃***, C***H₂***SAu), 1.74 (br, o, 6H, (C***H₂***)$_6$), 1.31 (br, o, 6H, (C***H₂***)$_6$).

^{13}C-NMR (ppm, $CDCl_3$, 75 MHz): δ 171.49 (N***C***N), 139.21, 138.74, 131.09,, 129.07, 128.29, 128.52, 128.29, 127.59, 127.05, 125.49, 124.98, 124.64, 120.80, 120.66, 117.61, 117.11, 116.83, 111.18, 109.59 (aromatic carbons and N***C***Cl***C***ClN), 73.13 (***C***HOH), 56.19 (N***C***H_2CH), 45.62 (N***C***H_2), 44.45 (S***C***H_2), 36.81 (N***C***H_3), 30.11, 28.82, 26.37 (***C***H_2 of alkyl chain), 20.43 (Ar-***C***H_3), 19.69 (Ar-***C***H_3).

Maldi-MS (CH_3CN) calcd/found (m/z): $[C_{34}H_{41}AuBrCl_2N_3OS]^+$ 885.1014/885.0797. Elemental Analysis: calculated for $C_{34}H_{40}AuBrCl_2N_3OS$ (886.54) C, 46.06; H, 4.55; N, 4.74. Found C, 46.06; H, 4.56; N, 4.75.

AuL10 - *((9-(6-bromo-1,4-dimethyl-9H-carbazol-9-yl)nonyl)thio)(4,5-dichloro-1-(2-hydroxy-2-phenylethyl)-3-methyl-1H-imidazol-2-yl)gold*

^{1}H-NMR (ppm, $CDCl_3$, 400MHz): δ 8.33 (s, 1H, aromatic hydrogen), 7.59-6.95 (o, 9H, aromatic hydrogens), 5.45 (m, 1H, C***H***OH), 4.52 (t, *J* 8 Hz, 2H, NC***H₂***), 4.39 (m, 2H, NC***H₂***CH), 3.90 (s, 3H, NC***H₃***), 2.87 (s, 3H, Ar-C***H₃***,), 2.83 (s, 3H, Ar-C***H₃***), 2.72 (t, *J* 8 Hz, 2H, C***H₂***SAu), 1.84 -1.35 (br, o, (C***H₂***)$_6$, 12H).

^{13}C-NMR (ppm, $CDCl_3$, 75 MHz): δ 171.49 (N***C***N), 139.21, 138.74, 131.09,, 129.07, 128.29, 128.52, 128.29, 127.59, 127.05, 125.49, 124.98, 124.64, 120.80, 120.66, 117.61, 117.11, 116.83, 111.18, 109.59 (aromatic carbons and N***C***Cl***C***ClN), 73.13 (***C***HOH), 56.19 (N***C***H_2CH), 45.62 (N***C***H_2), 44.45

(S***C***H_2), 39.13 (N***C***H_3) , 30.11, 29.30, 28.82, 27.91, 26.37 (***C***H_2 of alkyl chain), 20.43 (Ar-***C***H_3), 19.69 (Ar-***C***H_3).

Maldi-MS (CH_3CN) calcd/found (m/z): $[C_{35}H_{43}AuBrCl_2N_3OS]^+$ 899.1170/899.1175. Elemental Analysis: calculated for $C_{35}H_{42}AuBrCl_2N_3OS$ (900.57) C, 46.68; H, 4.70; N, 4.67. Found C, 46.69; H, 4.71; N, 4.66.

Synthesis of 7-(6-bromo-1,4-dimethyl-9H-carbazol-9-yl)heptane-1-thiolate dimethylsulfide gold (I) (AuCS3)

CS3, $N(CH_2CH_3)_3$ and dry dichloromethane were introduced in a Schlenk flask equipped with a magnetic stirrer. After 15 minutes, $(Me_2S)AuCl$ was added and the solution was stirred at room temperature for 4 hours in the dark. The solution was filtered, and the solvent was removed under reduced pressure. The yellow solid residue was washed with hexane (3x10 mL).

^{1}H-NMR (ppm, $CDCl_3$, 400 MHz): δ 8.25 (s, 1H, aromatic hydrogen), 7.51 (d, *J* 12 Hz, 1H, Ar-***H***), 7.26 (br d, 1H, Ar-***H***), 7.09 (d, *J* 8 Hz, 1H, Ar-***H***), 6.89 (d, *J* 8 Hz, 1H, Ar-***H***), 4.43 (br t, 2H, NC***H₂***), 3.11 (m, 6H, S(C***H₃***)$_2$), 2.79 (s, 3H, Ar-C***H₃***), 2.75 (s, 3H, Ar-C***H₃***), 2.63 (t, *J* 12 Hz, 2H, C***H₂***SAu), 1.76-1.40 (m, 10H, (C***H₂***)$_5$).

^{13}C-NMR (ppm, $CDCl_3$, 75 MHz): δ 139.38, 131.06, 128.99, 128.58, 127.04, 125.54, 124.95, 124.67, 120.65, 109.57 (aromatic carbons), 45.40 and 45.31 (S(***C***H_3)$_2$), 44.40 (S***C***H_2), 38.44 (N***C***H_2), 30.48, 30.10, 28.57, 27.81, 26.36 ((***C***H_2)$_5$), 20.43 (Ar-***C***H_3), 19.10 (Ar-***C***H_3).

Maldi-MS (CH_3CN) calcd/found (m/z): mass of the complex without a methyl group on the sulphur $[C_{22}H_{29}AuBrNS_2]^+$ 648.4710/648.3649. Elemental Analysis: calculated for $C_{23}H_{31}AuBrNS_2$ C, 41.70; H, 4.72; N, 2.11. Found C, 41.72; H, 4.71; N, 2.12.

Determination of the logarithm of the partition coefficient (LogP)

The logarithm of the partition coefficient (LogP) for **AuL10** was determined according to the following procedure. 100 mL of water (distilled after milli-Q purification) and 100 mL of 1-octanol were stirred together for 72h to allow saturation of both phases. Five standard solutions of complexes were prepared in the 1-octanol phase and other five in the water phase (20, 40, 60, 80 and 100 μM), and a calibration curve (absorbance vs concentration) was obtained using UV/vis spectroscopy. A further solution of both complexes was prepared in a 1-octanol phase (50 μM) and an equal volume

of water was added. The biphasic solutions were mixed for 20 minutes and then centrifuged for 1h at 6500 rpm to allow separation. Concentration in each phase was determined by UV/Vis. LogP was calculated using the following formula: log[complex]oct/[complex]H_2O. logP = 1.23

4.2.Docking studies

We used the three-dimensional structure of human iNOS determined by X-ray Crystallography [C1; PDB code 4UX6] [31] and the crystal structures of the human Topoisomerase I in covalent and noncovalent complexes with DNA [C2, PDB code 1A35] [45] as molecular targets for the docking simulations. The molecular structures of the three metallic compounds (**AuL8**, **AuL9** and **AuL10**) and Indometacine were built and energy minimized using the program MarvinSketch [ChemAxon ltd, Budapest, Hu]. To evaluate the possible binding modes of the indicated molecules to the proteins hTopoI and iNOS, and their different binding energies, we used the program suite Autodock v.4.2.2 [46]. The latter is a software tool that calculates a possible binding affinity constant (Ki) based on the binding energy between the target protein and the possible ligand, according to the expression Ki = exp (deltaG/ (R*T)). To rank the possible binding modes, we took into consideration the clusterization of the results from the simulations, as discussed in previous works [6, 24, 47-49]. Finally, the obtained best poses for each complex were visually examined to evaluate the quality of the protein:ligand interactions. In our approach, based on a "blind docking" strategy in all our simulations, the docking of the different compounds to the target protein has been done without any *a priori* knowledge of the binding site by the system. We used the standard default values as given by the program in each run. To prepare the protein and the ligands we used the ADT graphical interface [50]. We considered the ligands as fully flexible objects, and the protein target as full rigid in order to reduce the computational time. A cluster analysis based on root mean squares deviation (RMSD) values of each pose with respect to the starting geometry was performed. The lowest energetic conformation of the most populated cluster was considered as the best candidate. In case two or more clusters were almost equipopulated, keeping their energy distribution spread, the corresponding candidates were considered as bad ligands [51]. The binding modes resulting from our simulations were ranked on the basis of their binding energy values and subsequently clustered on the basis of a RMSD cut-off value of 2.0 Å. From the structural analysis of the lowest energy solutions of each cluster, we could spot the putative protein binding site. Figures 4 and 7, representative of the ligand:protein binding modes, were drawn using the program Chimera [52].

4.3.Biology

4.3.1.Cell cultures

All the cell lines used for the reported experiments were obtained from American Type Culture Collection (ATCC, Manassas, VA, USA). Human breast cancer cells MCF-7 and MDA-MB-231, human mammary epithelial cell line MCF-10A and mouse BALB/3T3 embryonic fibroblasts were maintained as described in [53, 54]. The murine macrophages RAW 264.7 were grown in Dulbecco's Modified Eagle's Medium (DMEM) high glucose (4.5 g/L), added with 10% Foetal Bovine Serum (FBS), 1% L-glutamine and 100 units/mL of penicillin/streptomycin [10]. All the cell cultures were grown at 37°C, in a humidified atmosphere containing 5% CO_2.

4.3.2.MTT assay

The 3-(4,5-dimethylthiazol-2-yl)-2,5-diphenyl-2H-tetrazolium bromide (MTT) assay (Sigma Aldrich (St. Louis, MO, USA)) was performed as previously reported [55]. Briefly, cells were treated for 72 h with 5 different concentrations of the given compound, then IC_{50} values were obtained through GraphPad Prism 9 software (GraphPad Software, La Jolla, CA, USA).

4.3.3.TUNEL Assay

The terminal deoxynucleotidyl transferase dUTP nick end labelling (TUNEL) assay was used for detecting DNA damage and cell death (CF™488A TUNEL Assay Apoptosis Detection Kit, Biotium, Hayward, CA, USA), as reported by [56] Nuclear staining was obtained using a DAPI solution (0.2 µg/mL, Sigma Aldrich, Milan, Italy). Leica DM 6000 fluorescence microscope was used for the observations (20 or 40x magnification, as indicated). Images were acquired and processed using LAS-X software. Each image is representative of three different experiments, representative fields are shown.

4.3.4.Human topoisomerase I relaxation assay

hTopo I relaxation assay was performed as reported in [57]. 0.25 µg of supercoiled plasmid pHOT1 in TE buffer (TopoGEN, Port Orange, FL, USA), tested complexes (at the indicated concentrations) and recombinant hTopo I (2 units, Topo- GEN, Port Orange, FL, USA) were mixed in a 20 µL final volume. The mixture was incubated for 1h at 37 °C, then loaded onto an 1% agarose gel containing 1x TAE buffer without ethidium bromide (EB) and run. At the end, agarose gel was stained (1x TAE buffer added with EB, 0.5 mg/mL, for 30 minutes) and washed (distilled water, three times for 5

minutes each). A UV transilluminator permitted the visualization. The image is representative of three different experiments.

4.3.5.Anti-inflammatory activity

The anti-inflammatory activity was tested by the means of the Griess assay on murine macrophages RAW 264.7, measuring the NO production, as reported by [10]. Briefly, cells were plated in 48 multi-wells then treated with the tested molecules, at the indicated concentrations and time, and the lipopolysaccharide (LPS, Sigma Aldrich, Milan, Italy) at the final concentration of 1 µg/mL was used to induce inflammation and stimulate NO production. Next, cell medium and Griess reagent (Sigma Aldrich, Milan, Italy) were mixed (1:1 ratio) and left under agitation (30 minutes), then the absorbance at 540 nm was measured by the means of a multiplate reader. The absorbance values were used for calculating the NO production %.

4.2.6.Immunofluorescence

Cells were grown on glass coverslips in full medium, then serum-deprived for 24 h and treated with the complexes at the indicated concentrations and time. Next, cells were PBS-washed and fixed using cold methanol (15 min, -20 °C). Primary antibodies raised against NF-κB, iNOS, TNF-α, (Santa Cruz Biotechnology Inc., CA, USA) diluted in BSA 2%, were added and incubated overnight, (4 °C) as described in [10]. Alexa Fluor®568 conjugate goat-anti-mouse (1:500 dilution, from Thermo Fisher Scientific, MA, USA) was used as secondary antibody. DAPI (Sigma Aldrich, Milan, Italy) 0.2 µg/mL was used for nuclei counterstain (10 min). A Leica DM 6000 fluorescence microscope was used to visualize the images. The LAS-X software was adopted for images acquisition and processing. Image J software was used for fluorescence quantification.

4.3.7.Antioxidant Activity

The antioxidant activity was determined on fibroblasts BALB/3T3 using $DCFH_2$-DA, as already described [54]. In short, the murine BALB/3T3 fibroblasts were plated (white 96 MW), treated with the compounds as indicated, then Menadione (Men, 25 µM) was added for 15 minutes. Next, cells were PBS-washed and treaded with 25 µM 2′-7′-dichlorofluorescein diacetate ($DCFH_2$-DA, Sigma-Aldrich) for 40 min at 37 °C and 5% CO_2. Finally, cells were PBS-washed and the fluorescence was detected using a multiplate reader (λ_{ex}= 485 nm, λ_{em}= 535 nm).

ROS production inhibition % (I_{ROS}) *vs* Men was calculated using the following formula:

$$I_{ROS}\ vs\ Men\ (\%) = \frac{F_{Men} - F_{Sample}}{F_{Men}} * 100$$

where F_{Men} is the mean fluorescence after treatment with Men alone and F_{sample} the mean fluorescence after the co-treatment complexes/ Men.

4.3.8.Statistical analysis

One-way ANOVA followed by Dunnett's multiple comparison test performed by GraphPad Prism 9 was employed to analyze data for statistical significance, as indicated. Standard deviations are shown.

Authors Contributions: Conceptualization: M. S. Sinicropi, P. Longo; Data curation: A. D'Amato, D. Iacopetta, A. Mariconda, A. Catalano; Formal analysis: J. Ceramella, M. Marra, C. Rosano; Funding acquisition: A. D'Amato, A. Mariconda, M. S. Sinicropi, P. Longo; Investigation: A. D'Amato, D. Iacopetta, J. Ceramella, M. Marra, R. Troiano; Methodology: A. D'Amato, D. Iacopetta, A. Mariconda, R. Troiano. C. Saturnino; Project administration: M. S. Sinicropi, P. Longo; Resources; A. Mariconda, M. S. Sinicropi, P. Longo; Software: D. Iacopetta, J. Ceramella, C. Rosano; Supervision: A. Catalano, M. S. Sinicropi, P. Longo; Validation: D. Iacopetta, A. Mariconda, A.; Visualization: J. Ceramella, M. Marra, R. Troiano, C. Saturnino, C. Rosano; Writing - original draft: D'Amato, D. Iacopetta, A. Mariconda; A. Writing - review & editing: M. S. Sinicropi, P. Longo.

Funding: This work was supported by PRIN 2022 PNRR, Code P20222BLAZ − Enhanced pharmacological activity of noble metal carbene-N-heterocyclic complexes by oligopeptide counterion (CUP MASTER: D53D23016900001) and PRIN 2022, Code 2022HARH5W − HyMTA (Hybrid Multi-Target Agents) (CUP MASTER: C53D23004490001).

Declaration of competing interest: The authors declare that they have no known competing financial interests or personal relationships that could have appeared to influence the work reported in this paper.

Data availability All data has been included in this submission.

Acknowledgement: Patrizia Oliva and Patrizia Iannece are acknowledged for technical assistance.

Supplementary data to this article can be found online at

References

[1] Shaveta, S. Mishra, P. Singh, Hybrid molecules: The privileged scaffolds for various pharmaceuticals, European Journal of Medicinal Chemistry, 124 (2016) 500-536.
[2] L.F. Tietze, H.P. Bell, S. Chandrasekhar, Natural Product Hybrids as New Leads for Drug Discovery, Angewandte Chemie International Edition, 42 (2003) 3996-4028.
[3] A.H. Alkhzem, T.J. Woodman, I.S. Blagbrough, Design and synthesis of hybrid compounds as novel drugs and medicines, RSC Advances, 12 (2022) 19470-19484.
[4] C. Saturnino, D. Iacopetta, M. Sinicropi, C. Rosano, A. Caruso, A. Caporale, N. Marra, B. Marengo, M. Pronzato, O. Parisi, P. Longo, R. Ricciarelli, N-Alkyl Carbazole Derivatives as New Tools for Alzheimer's Disease: Preliminary Studies, Molecules, 19 (2014) 9307-9317.
[5] D. Iacopetta, C. Rosano, M. Sirignano, A. Mariconda, J. Ceramella, M. Ponassi, C. Saturnino, M.S. Sinicropi, P. Longo, Is the Way to Fight Cancer Paved with Gold? Metal-Based Carbene Complexes with Multiple and Fascinating Biological Features, Pharmaceuticals, 13 (2020).
[6] M.S. Sinicropi, D. Iacopetta, C. Rosano, R. Randino, A. Caruso, C. Saturnino, N. Muià, J. Ceramella, F. Puoci, M. Rodriquez, P. Longo, M.R. Plutino, N-thioalkylcarbazoles derivatives as new anti-proliferative agents: synthesis, characterisation and molecular mechanism evaluation, Journal of Enzyme Inhibition and Medicinal Chemistry, 33 (2018) 434-444.
[7] J. Ceramella, A. Mariconda, M. Sirignano, D. Iacopetta, C. Rosano, A. Catalano, C. Saturnino, M.S. Sinicropi, P. Longo, Novel Au Carbene Complexes as Promising Multi-Target Agents in Breast Cancer Treatment, Pharmaceuticals, 15 (2022).
[8] D. Iacopetta, J. Ceramella, C. Rosano, A. Mariconda, M. Pellegrino, M. Sirignano, C. Saturnino, A. Catalano, S. Aquaro, P. Longo, M.S. Sinicropi, N-Heterocyclic Carbene-Gold(I) Complexes Targeting Actin Polymerization, Applied Sciences, 11 (2021).
[9] J. Ceramella, D. Iacopetta, A. Caruso, A. Mariconda, A. Petrou, A. Geronikaki, C. Rosano, C. Saturnino, A. Catalano, P. Longo, M.S. Sinicropi, 5,8-Dimethyl-9H-carbazole Derivatives Blocking hTopo I Activity and Actin Dynamics, Pharmaceuticals, 16 (2023).
[10] A. Mariconda, D. Iacopetta, M. Sirignano, J. Ceramella, A. D'Amato, M. Marra, M. Pellegrino, M.S. Sinicropi, S. Aquaro, P. Longo, Silver and Gold Complexes with NHC-Ligands Derived from Caffeine: Catalytic and Pharmacological Activity, International Journal of Molecular Sciences, 25 (2024).
[11] D. Iacopetta, C. Costabile, M. La Chimia, A. Mariconda, J. Ceramella, D. Scumaci, A. Catalano, C. Rosano, G. Cuda, M.S. Sinicropi, P. Longo, NHC-Ag(I) and NHC-Au(I) Complexes with N-Boc-Protected α-Amino Acidate Counterions Powerfully Affect the Growth of MDA-MB-231 Cells, ACS Medicinal Chemistry Letters, 14 (2023) 1567-1575.
[12] A. Głuszyńska, Biological potential of carbazole derivatives, European Journal of Medicinal Chemistry, 94 (2015) 405-426.
[13] J. Ceramella, A. Mariconda, D. Iacopetta, C. Saturnino, A. Barbarossa, A. Caruso, C. Rosano, M.S. Sinicropi, P. Longo, From coins to cancer therapy: Gold, silver and copper complexes targeting human topoisomerases, Bioorganic & Medicinal Chemistry Letters, 30 (2020).
[14] A. Mariconda, M. Sirignano, R. Troiano, S. Russo, P. Longo, N-Heterocyclic Carbene Gold Complexes Active in Hydroamination and Hydration of Alkynes, Catalysts, 12 (2022).
[15] J. Ceramella, D. Iacopetta, A. Barbarossa, A. Caruso, F. Grande, M.G. Bonomo, A. Mariconda, P. Longo, S. Carmela, M.S. Sinicropi, Carbazole Derivatives as Kinase-Targeting Inhibitors for Cancer Treatment, Mini-Reviews in Medicinal Chemistry, 20 (2020) 444-465.
[16] S.A. Patil, S.A. Patil, E.A. Ble-González, S.R. Isbel, S.M. Hampton, A. Bugarin, Carbazole Derivatives as Potential Antimicrobial Agents, Molecules, 27 (2022).
[17] M. Napoli, C. Saturnino, E.I. Cianciulli, M. Varcamonti, A. Zanfardino, G. Tommonaro, P. Longo, Silver(I) N-heterocyclic carbene complexes: Synthesis, characterization and antibacterial activity, Journal of Organometallic Chemistry, 725 (2013) 46-53.
[18] C. Saturnino, I. Barone, D. Iacopetta, A. Mariconda, M.S. Sinicropi, C. Rosano, A. Campana, S. Catalano, P. Longo, S. Andò, N-heterocyclic carbene complexes of silver and gold as novel tools against breast cancer progression, Future Medicinal Chemistry, 8 (2016) 2213-2229.

[19] H.M.J. Wang, I.J.B. Lin, Facile Synthesis of Silver(I)−Carbene Complexes. Useful Carbene Transfer Agents, Organometallics, 17 (1998) 972-975.
[20] Q.-X. Liu, Z.-L. Hu, S.-C. Yu, Z.-X. Zhao, D.-C. Wei, H.-L. Li, NHC Pd(II) and Ag(I) Complexes: Synthesis, Structure, and Catalytic Activity in Three Types of C–C Coupling Reactions, ACS Omega, 3 (2018) 4035-4047.
[21] A. Mariconda, F. Grisi, C. Costabile, S. Falcone, V. Bertolasi, P. Longo, Synthesis, characterization and catalytic behaviour of a palladium complex bearing a hydroxy-functionalized N-heterocyclic carbene ligand, New J. Chem., 38 (2014) 762-769.
[22] P. Ai, M. Mauro, L. De Cola, A.A. Danopoulos, P. Braunstein, A Bis(Diphosphanyl N-Heterocyclic Carbene) Gold Complex: A Synthon for Luminescent Rigid AuAg2 Arrays and Au5 and Cu6 Double Arrays, Angewandte Chemie International Edition, 55 (2016) 3338-3341.
[23] L. Canovese, F. Visentin, C. Levi, V. Bertolasi, Synthesis and Mechanism of Formation of Novel NHC−NAC Bis-Carbene Complexes of Gold(I), Organometallics, 30 (2011) 875-883.
[24] D. Iacopetta, A. Mariconda, C. Saturnino, A. Caruso, G. Palma, J. Ceramella, N. Muià, M. Perri, M.S. Sinicropi, M.C. Caroleo, P. Longo, Novel Gold and Silver Carbene Complexes Exert Antitumor Effects Triggering the Reactive Oxygen Species Dependent Intrinsic Apoptotic Pathway, ChemMedChem, 12 (2017) 2054-2065.
[25] A. Mariconda, M. Sirignano, C. Costabile, P. Longo, New NHC- silver and gold complexes active in A3-coupling (aldehyde-alkyne-amine) reaction, Molecular Catalysis, 480 (2020).
[26] R. Mirzayans, D. Murray, Do TUNEL and Other Apoptosis Assays Detect Cell Death in Preclinical Studies?, International Journal of Molecular Sciences, 21 (2020).
[27] J. Moon, I. Kitty, K. Renata, S. Qin, F. Zhao, W. Kim, DNA Damage and Its Role in Cancer Therapeutics, International Journal of Molecular Sciences, 24 (2023).
[28] R. Wang, Y. Sun, C. Li, Y. Xue, X. Ba, Targeting the DNA Damage Response for Cancer Therapy, International Journal of Molecular Sciences, 24 (2023).
[29] P.A. Yakkala, N.R. Penumallu, S. Shafi, A. Kamal, Prospects of Topoisomerase Inhibitors as Promising Anti-Cancer Agents, Pharmaceuticals, 16 (2023).
[30] Y. Pommier, J.M. Barcelo, V.A. Rao, O. Sordet, A.G. Jobson, L. Thibaut, Z.H. Miao, J.A. Seiler, H. Zhang, C. Marchand, K. Agama, J.L. Nitiss, C. Redon, Repair of Topoisomerase I-Mediated DNA Damage, in, 2006, pp. 179-229.
[31] D.R. Cheshire, A. Åberg, G.M.K. Andersson, G. Andrews, H.G. Beaton, T.N. Birkinshaw, N. Boughton-Smith, S. Connolly, T.R. Cook, A. Cooper, S.L. Cooper, D. Cox, J. Dixon, N. Gensmantel, P.J. Hamley, R. Harrison, P. Hartopp, H. Käck, P.D. Leeson, T. Luker, A. Mete, I. Millichip, D.J. Nicholls, A.D. Pimm, S.A. St-Gallay, A.V. Wallace, The discovery of novel, potent and highly selective inhibitors of inducible nitric oxide synthase (iNOS), Bioorganic & Medicinal Chemistry Letters, 21 (2011) 2468-2471.
[32] R. Zamora, Y. Vodovotz, T.R. Billiar, Inducible Nitric Oxide Synthase and Inflammatory Diseases, Molecular Medicine, 6 (2000) 347-373.
[33] P. Rapisarda, G. Frasca, A.M. Panico, F. Bonina, R. Messina, L. Rizza, G. Musumeci, V. Cardile, Involvement of inducible nitric oxide synthase and cyclooxygenase-2 in the anti-inflammatory effects of a red orange extract in human chondrocytes, Natural Product Research, 24 (2010) 1469-1480.
[34] F. Vannini, K. Kashfi, N. Nath, The dual role of iNOS in cancer, Redox Biology, 6 (2015) 334-343.
[35] K. Taniguchi, M. Karin, NF-κB, inflammation, immunity and cancer: coming of age, Nature Reviews Immunology, 18 (2018) 309-324.
[36] T. Zhang, C. Ma, Z. Zhang, H. Zhang, H. Hu, NF-κB signaling in inflammation and cancer, MedComm, 2 (2021) 618-653.
[37] M. Barkett, T.D. Gilmore, Control of apoptosis by Rel/NF-κB transcription factors, Oncogene, 18 (1999) 6910-6924.
[38] R.E. Simmonds, B.M. Foxwell, Signalling, inflammation and arthritis: NF- B and its relevance to arthritis and inflammation, Rheumatology, 47 (2008) 584-590.
[39] Y. Wu, B.P. Zhou, TNF-α/NF-κB/Snail pathway in cancer cell migration and invasion, British Journal of Cancer, 102 (2010) 639-644.
[40] H. Wajant, P. Scheurich, TNFR1-induced activation of the classical NF-κB pathway, The FEBS Journal, 278 (2011) 862-876.

[41] M.A. Tan, N. Sharma, S.S.A. An, Phyto-Carbazole Alkaloids from the Rutaceae Family as Potential Protective Agents against Neurodegenerative Diseases, Antioxidants, 11 (2022).
[42] M. Mora, M.C. Gimeno, R. Visbal, Recent advances in gold–NHC complexes with biological properties, Chemical Society Reviews, 48 (2019) 447-462.
[43] H.J. Forman, H. Zhang, Targeting oxidative stress in disease: promise and limitations of antioxidant therapy, Nature Reviews Drug Discovery, 20 (2021) 689-709.
[44] Q.-Q. Wu, Q.-H. Song, Photosensitized Splitting of Thymine Dimer or Oxetane Unit by a Covalently N-Linked Carbazole via Electron Transfer in Different Marcus Regions, The Journal of Physical Chemistry B, 114 (2010) 9827-9832.
[45] M.R. Redinbo, L. Stewart, P. Kuhn, J.J. Champoux, W.G.J. Hol, Crystal Structures of Human Topoisomerase I in Covalent and Noncovalent Complexes with DNA, Science, 279 (1998) 1504-1513.
[46] G.M. Morris, R. Huey, W. Lindstrom, M.F. Sanner, R.K. Belew, D.S. Goodsell, A.J. Olson, AutoDock4 and AutoDockTools4: Automated docking with selective receptor flexibility, Journal of Computational Chemistry, 30 (2009) 2785-2791.
[47] M.F. Santolla, E.M. De Francesco, R. Lappano, C. Rosano, S. Abonante, M. Maggiolini, Niacin activates the G protein estrogen receptor (GPER)-mediated signalling, Cellular Signalling, 26 (2014) 1466-1475.
[48] N. Abbassi, E.M. Rakib, H. Chicha, L. Bouissane, A. Hannioui, C. Aiello, R. Gangemi, P. Castagnola, C. Rosano, M. Viale, Synthesis and Antitumor Activity of Some Substituted Indazole Derivatives, Archiv der Pharmazie, 347 (2014) 423-431.
[49] C. Rosano, M. Ponassi, M.F. Santolla, A. Pisano, L. Felli, A. Vivacqua, M. Maggiolini, R. Lappano, Macromolecular Modelling and Docking Simulations for the Discovery of Selective GPER Ligands, The AAPS Journal, 18 (2015) 41-46.
[50] M.F. Sanner, B.S. Duncan, C. J.Carrillo, A.J. Olson, Integrating Computation and Visualization for Biomolecular Analysis: An Example Using Python and Avs, in: Biocomputing '99, 1998, pp. 401-412.
[51] C. Rosano, R. Lappano, M. F. Santolla, M. Ponassi, A. Donadini, M. Maggiolini, Recent Advances in the Rationale Design of GPER Ligands, Current Medicinal Chemistry, 19 (2012) 6199-6206.
[52] E.F. Pettersen, T.D. Goddard, C.C. Huang, G.S. Couch, D.M. Greenblatt, E.C. Meng, T.E. Ferrin, UCSF Chimera—A visualization system for exploratory research and analysis, Journal of Computational Chemistry, 25 (2004) 1605-1612.
[53] M.S. Sinicropi, J. Ceramella, P. Vanelle, D. Iacopetta, C. Rosano, O. Khoumeri, S. Abdelmohsen, W. Abdelhady, H. El-Kashef, Novel Thiazolidine-2,4-dione-trimethoxybenzene-thiazole Hybrids as Human Topoisomerases Inhibitors, Pharmaceuticals, 16 (2023).
[54] J. Ceramella, M.R. Loizzo, D. Iacopetta, M. Bonesi, V. Sicari, T.M. Pellicanò, C. Saturnino, A. Malzert-Fréon, R. Tundis, M.S. Sinicropi, Anchusa azurea Mill. (Boraginaceae) aerial parts methanol extract interfering with cytoskeleton organization induces programmed cancer cells death, Food & Function, 10 (2019) 4280-4290.
[55] D. Iacopetta, A. Fazio, C. La Torre, A. Barbarossa, J. Ceramella, F. Francomano, C. Saturnino, H. El-Kashef, S. Alcaro, M.S. Sinicropi, Annona cherimola Mill. Leaf Extracts Affect Melanoma Cells Growth and Progression, Foods, 11 (2022).
[56] J. Ceramella, R. Troiano, D. Iacopetta, A. Mariconda, M. Pellegrino, A. Catalano, C. Saturnino, S. Aquaro, M.S. Sinicropi, P. Longo, Synthesis of Novel N-Heterocyclic Carbene-Ruthenium (II) Complexes, “Precious” Tools with Antibacterial, Anticancer and Antioxidant Properties, Antibiotics, 12 (2023).
[57] A. Mariconda, D. Iacopetta, M. Sirignano, J. Ceramella, C. Costabile, M. Pellegrino, C. Rosano, A. Catalano, C. Saturnino, H. El-Kashef, S. Aquaro, M.S. Sinicropi, P. Longo, N-Heterocyclic Carbene (NHC) Silver Complexes as Versatile Chemotherapeutic Agents Targeting Human Topoisomerases and Actin, ChemMedChem, 17 (2022).